applied sciences

MDPI

Article

Dual-Targeting Gold Nanoparticles: Simultaneous Decoration with Ligands for Co-Transporters SGLT-1 and B^0AT1

Giuseppe D'Orazio [1,*], Marco Marradi [2] and Barbara La Ferla [3,*]

[1] Department of Chemistry, Università degli Studi di Milano, Via C. Golgi 19, 20133 Milan, Italy
[2] Department of Chemistry "Ugo Schiff", Università degli Studi di Firenze, Via della Lastruccia 13, 50019 Sesto Fiorentino, Italy; marco.marradi@unifi.it
[3] Department of Earth and Environmental Sciences DISAT, Università degli Studi di Milano-Bicocca, Piazza della Scienza 1, 20126 Milan, Italy
* Correspondence: giuseppe.dorazio@unimi.it (G.D.); barbara.laferla@unimib.it (B.L.F.)

Abstract: Sodium–glucose co-transporter 1 (SGLT1) and sodium-dependent neutral amino acid transporter (B^0AT1) are mainly expressed on the membrane of enterocytes, a type of epithelial cell found in the intestines. In addition to their physiological role in the absorption of nutrients, a protective role in the integrity of the intestinal barrier has been established. The natural ligands of SGLT1 (D-glucose) and of B^0AT1 (L-glutamine) can trigger a protective anti-inflammatory effect on the intestinal epithelium. The literature suggests the activation of common intracellular pathways upon engagement of the two transporters, whose functional forms are composed of oligomers or clusters. Simultaneous activation of these two co-transporters could lead to a potential multitarget and synergistic anti-inflammatory effect. Therefore, nanoplatforms containing multiple copies of the ligands could represent chemical tools to study the potential simultaneous activation of the two co-transporters. For these reasons, in this study, a set of different gold nanoparticles decorated with derivatives of D-glucose and of L-glutamine were designed and prepared. In particular, the synthesis of suitable sulfur-ending functionalized ligand derivatives, including a *C*-glucoside derivative, their anchoring to gold nanoparticles and their physical–chemical characterization have been carried out. The obtained nanostructures could represent promising multifunctional platforms for further investigation of the existence of possible multitarget and synergistic effects toward the two co-transporters SGLT1 and B^0AT1.

Keywords: gold nanoparticles; multivalency; sodium–glucose co-transporter 1 (SGLT1); sodium–glutamine co-transporter 1 (B^0AT1); glycoderivatives; thiol–ene coupling

Citation: D'Orazio, G.; Marradi, M.; La Ferla, B. Dual-Targeting Gold Nanoparticles: Simultaneous Decoration with Ligands for Co-Transporters SGLT-1 and B^0AT1. *Appl. Sci.* **2024**, *14*, 2248. https://doi.org/10.3390/app14062248

Academic Editor: Alfonso Zambon

Received: 23 January 2024
Revised: 3 March 2024
Accepted: 5 March 2024
Published: 7 March 2024

1. Introduction

The key role of the intestine in the maintenance of body homeostasis as well as in the regulation and control of the immune response to pathogens is nowadays an unquestionable scientific fact, supported by many relevant studies in the field of immunology and pathophysiology [1–6]. Several studies published in the last two decades have demonstrated that D-glucose, administered at high concentrations in vitro to intestinal epithelial cells (IECs) and in vivo in mice (oral administration), has a protective effect against cell/tissue damages caused by pathogens expressing lipopolysaccharides (LPSs) [7,8]. These studies propose that the mechanism of the glucose-mediated cytoprotective effect depends on increased glucose uptake by enterocytes, mediated by sodium–glucose co-transporter 1 (SGLT1). The unidirectional translocation of glucose from the intestinal lumen to the cytoplasm of IECs, mediated by this transmembrane protein, represents one of the principal mechanisms for the absorption of glucose occurring on the brush border membrane in the gut [9–11].

More recently, other works have outlined the protective effect of SGLT1 engagement with high oral doses of D-glucose and non-metabolizable 3-*O*-methyl-D-glucopyranose

duced mucositis [15]. Our previous results suggested that C-glucoside **1** mediates a protective activity, similar to that observed for D-glucose, due to its agonistic interaction with SGLT1. This binding produces an activated form of the transporter, which activates an intracellular signaling pathway that ultimately results in protective and anti-inflammatory effects.

On the other hand, L-glutamine (Figure 1) is the most abundant amino acid in the total body free amino acid pool, and recently, its role in nutrition is receiving growing interest. L-glutamine is a major energy source for the intestinal epithelium, and it is involved in the maintenance of intestinal epithelial homeostasis. In fact, L-glutamine represents an important supplement in diets within therapeutic supportive care protocols; its enrichment in parenteral hyperalimentation can decrease villus atrophy associated with exclusive parenteral feeding [16–18]. The protective anti-inflammatory effects of glutamine are also well established [19,20]. For example, diet supplementation with glutamine may protect the intestinal tract from radiation and some chemotherapeutic agents. In animal models of gastrointestinal mucositis, oral glutamine treatment mitigates mucosal damage and enhances intestinal recovery after chemotherapy-induced injury [21–24]. For example, studies have shown that orally administering L-glutamine can prevent gut mucosal injuries caused by cisplatin in rats. Additionally, this drug upregulates L-glutamine transport in human intestinal epithelial cells, potentially leading to increased intracellular levels of glutathione (GSH) [25,26].

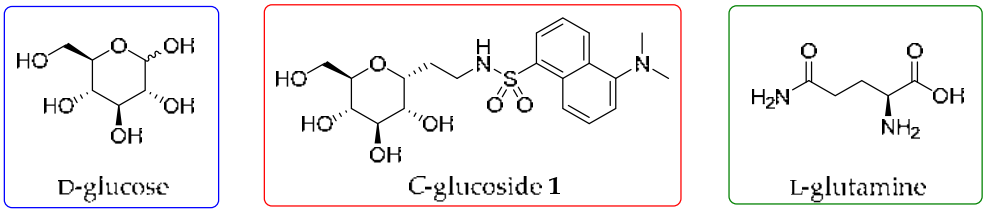

Figure 1. Structure of the three monomeric ligands with known activity toward SGLT1 and B^0AT1: D-glucose, C-glucoside **1** and L-glutamine.

Similarly to D-glucose, the absorption of L-glutamine by the intestinal epithelium is mediated by several transport systems, among which sodium–glutamine cotransporter 1 (B^0AT1) is the main transmembrane protein that mediates the absorption of L-glutamine by villus enterocytes [27]. One of the critical events compromising the biological functions of the intestinal epithelium—such as nutrient absorption and the barrier effect against pathogen invasion—is the disruption of the correct permeability due to alterations in the junctional systems of epithelial cells in response to various forms of damage [28,29]. The fundamental link between SGLT1 activation and L-glutamine uptake is the ability to modulate tight junctions activating intracellular signaling pathways involved in junctional open–close mechanisms and remodeling [30–34]. Thus, the simultaneous activation of both receptors could be of great relevance, as it could lead to a multitarget and synergistic protective effect.

Moreover, both SGLT1 and B^0AT1 co-transporters have been described to be involved in anti-inflammatory and anti-apoptotic signaling in the repair of plasma membrane integrity and tight junction integrity, thus representing potential molecular targets for a

Moreover, both SGLT1 and B^0AT1 co-transporters have been described to be involved in anti-inflammatory and anti-apoptotic signaling in the repair of plasma membrane integrity and tight junction integrity, thus representing potential molecular targets for a therapeutic approach aimed at the prevention of intestinal barrier damages and/or its recovery [35].

Several reports have suggested that functional SGLT1 is an oligomeric protein resulting from the homodimerization of two identical subunits [36–39]. The evidence also suggests that the B^0AT1 transporter is mainly assembled as a cluster [40], and the B^0AT1 transporter localized in the small intestine displays a low-affinity constant for the amino acid substrate [40]. These findings suggest that the study of multitarget and multivalent effects of the ligand *C*-glycoside **1** or L-glutamine could lead to a significant increase in the activity.

Multivalent binding is a commonly observed process in biological systems, in particular during cellular recognition events and in signal transduction pathways. Multivalent interactions are significantly stronger than the individual binding of an equal amount of monovalent ligands to a multivalent receptor [41,42]. Receptor dimerization/clustering is a well-known and ubiquitous phenomenon.

Gold nanoparticles (AuNPs) are one of the most used nanoplatforms for the study of multivalency phenomena, owing to their good stability, unique optical features, and ease and versatility in decoration/functionalization with multiple copies of thiol-bearing ligands on the gold surface [43–48]. In particular, Glyco-Gold Nanoparticles (GAuNPs), i.e., AuNPs decorated with carbohydrates, are receiving increasing attention thanks to their marked potentialities in biomedicine [49], for the study of carbohydrate-mediated interactions involved in biochemical and physiological processes [50,51], for diagnostics [52,53], for the investigation of multivalency effects on sugars [54,55], including the modulation of enzyme activity [54,56], and as promising platforms for vaccine development [57–59]. Furthermore, the simultaneous introduction of different thiol-ligands on the same gold nanoplatform paves the way for "multifunctional" nanosystems [55,57].

Therefore, we reasoned that GAuNPs displaying multiple copies of SGLT1 and B^0AT1 ligands could be suitable nanotools for modulating the activity of these co-receptors. In the present article, AuNPs decorated with thiol-ending D-glucose derivatives (a β-*O*-alkylglucose derivative and *C*-glucoside **1**) and/or L-glutamine derivatives were prepared and fully characterized. These nanosized tools could be used for future studies aimed at evaluating the multivalent and synergistic effects on the target proteins SGLT1 and B^0AT1 (Figure 2).

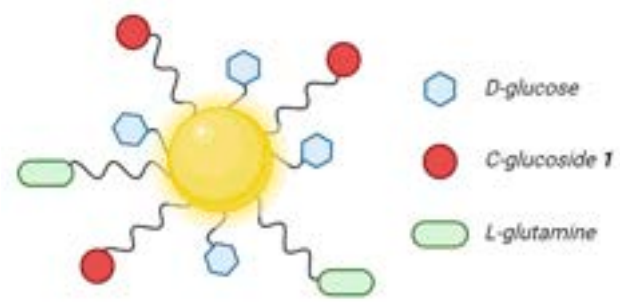

Figure 2. General scheme of the designed nanoplatforms decorated with the ligands of interest of this work (D-glucose, *C*-glucoside **1** and L-glutamine).

2. Materials and Methods

2.1. General Remarks

All commercial chemicals were purchased from Merck and Alfa Aesar. All chemicals were used without further purification. Thin layer chromatography (TLC) was performed on silica gel 60 F254 plates (Merck©, Darmstadt, Germany) with detection under UV light when possible, or by charring with a solution of $(NH_4)_6Mo_7O_{24}$ (21 g), $Ce(SO_4)_2$ (1 g), concentrated H_2SO_4 (31 mL) in water (500 mL) or with an ethanol solution of ninhydrin. Flash-column chromatography was performed on silica gel 230–400 mesh (Merck) or on an Isolera Flash Chromatography System (Biotage Sweden AB™, Uppsala, Sweden). ^1H and

^{13}C NMR spectra were recorded at 25 °C, unless otherwise stated, with a Varian Mercury 400 MHz instrument (Varian Inc., Palo Alto, CA, USA), on a Bruker DRX-300 spectrometer and on Bruker AvanceTM NEO 400 MHz (Bruker©, Billerica, MA, USA). Chemical shift assignments, reported in parts per million, were referenced to the corresponding solvent peaks. Mass spectra were recorded on an ABSciex 2000 QTRAP LC/MS/MS system with an ESI source (ABSciex©, Framingham, MA, USA). TEM examination was carried out at 200 KeV with a Philips CM200 microscope (Philips©, Amsterdam, The Netherlands). UV spectra were obtained with a UV/vis Perkin-Elmer Lambda 12 spectrophotometer (Perkin-Elmer©, Waltham, MA, USA). Infrared spectroscopy analyses were performed in ATR mode using a Jasco© FT/IR-4600 system ((Jasco Europe©, Cremella, Italy).

2.2. Synthesis of Ligands

2.2.1. Synthesis of C-Glucoside Derivative **2**

For compounds **6** and **7**, synthetic procedures and characterizations are already reported in [60,61].

2.2.2. 2,3,4-Tri-O-benzyl-6-O-acetyl-α-C-allyl-glucopyranoside **8**

A mixture of Ac_2O/trifluoroacetic acid 4:1 (70 mL), prepared at 0 °C in argon atmosphere, was added via a double-tip needle to a round-bottomed flask containing 2 g (3.55 mmol) of 2,3,4,6-tetra-*O*-benzyl-α-D-glucopyranose **7**. The solution was stirred vigorously at 0 °C and the reaction followed by TLC (Hexane/EtOAc 8.5:1.5). After 1.5 h, no more starting compound was present, and the solution was gently poured into ice water and stirred for 10 min. The aqueous solution was extracted with EtOAc (3×), the organic phase was then washed once with a sodium hydrogen carbonate saturated solution and twice with distilled water. The organic phase was dried over sodium sulfate, filtered and concentrated. The resulting crude was purified by flash chromatography (silica gel, eluent: Hexane/EtOAc 9:1), affording compound **8** (1.61 g, 3.12 mmol, 88% yield).

^{1}H NMR (400 MHz, $CDCl_3$) δ 7.43–7.24 (m, 15H, C*H* Ar), 5.79 (ddt, J = 17.2, 10.2, 6.9 Hz, 1H, H2′), 5.18–5.05 (m, 2H, H3′a,b), 4.98 (d, J = 10.8 Hz, 1H, CH_2Ph), 4.89 (d, J = 10.7 Hz, 1H, CH_2Ph), 4.83 (d, J = 10.8 Hz, 1H, CH_2Ph), 4.72 (d, J = 11.6 Hz, 1H, CH_2Ph), 4.65 (d, J = 11.6 Hz, 1H, CH_2Ph), 4.57 (d, J = 10.8 Hz, 1H, CH_2Ph), 4.24 (d, J = 3.5 Hz, 2H, H6a,b), 4.11 (dt, J = 9.3, 5.9 Hz, 1H, H1, H1), 3.85 (t, J = 9.0 Hz, 1H, H3), 3.76 (dd, J = 9.4, 5.8 Hz, 1H, H2), 3.70 (dt, J = 9.8, 3.5 Hz, 1H, H5), 3.48 (dd, J = 9.8, 8.7 Hz, 1H, H4), 2.50 (t, J = 8.2 Hz, 2H, H1′a,b) and 2.04 (s, 3H, CH_3CO).

^{13}C NMR (101 MHz, $CDCl_3$) δ 170.92 (CH_3CO), 138.59 (Cq Ar), 138.15 (Cq Ar), 137.83 (Cq Ar), 134.40 (C2′), 128.80, 128.65, 128.59, 128.58, 128.49, 128.29, 128.11, 128.05, 128.00, 127.95 and 127.85 (C Ar × 15), 117.24 (C3′), 82.37 (C3), 80.04 (C2), 77.89 (C4), 75.65 and 75.21 (CH_2Ph), 73.68 (C1), 73.23 (CH_2Ph), 69.68 (C5), 63.62 (C6), 29.89 (C1′) and 21.00 (CH_3CO).

MS: m/z = 517.6 $[M+H]^+$.

2.2.3. 2-(2,3,4-Tri-O-benzyl-6-acetyl-α-D-glucopyranosyl)-ethanal **9**

To a solution of **8** (3.53 g, 6.84 mmol) in CH_2Cl_2 (100 mL, 0.07 M) at −78 °C, O_3 was bubbled until a pale blue color appeared. The reaction was followed by TLC (Hexane/EtOAc 8:2). At the end of the reaction, the excess of O_3 was removed by purging the mixture with a stream of argon at −78 °C and then Ph_3P (17.1 mmol, 2.5 eq) was added. The mixture was stirred for 24 h at room temperature and then concentrated by rotary evaporation. The product was purified from the crude reaction by flash chromatography (silica gel, eluent: Hexane/EtOAc 8:2 to 7:3), affording aldehyde **9** (2.92 g, 5.63 mmol, 82% yield).

^{1}H NMR (400 MHz, $CDCl_3$) δ 9.72 (s, 1H, H2′ (CHO)), 7.43–7.24 (m, 15H, CH Ar), 4.93 (d, J = 10.9 Hz, 1H, CH_2Ph), 4.87 (d, J = 10.8 Hz, 1H, CH_2Ph), 4.83 (d, J = 10.9 Hz, 1H, CH_2Ph), 4.75–4.66 (m, 2H, CH_2Ph, H1), 4.63 (d, J = 11.5 Hz, 1H, CH_2Ph), 4.58 (d, J = 10.8 Hz, 1H, CH_2Ph), 4.30–4.18 (m, 2H, H6), 3.82–3.74 (m, 2H, H2, H3), 3.74–3.63 (m, 1H, H5),

3.53–3.43 (m, 1H, H4), 2.89 (dd, J = 15.8, 5.0 Hz, 1H, H1′a), 2.74 (ddd, J = 16.2, 8.6, 2.8 Hz, 1H, H1′b) and 2.05 (s, 3H, CH_3CO).

^{13}C NMR (101 MHz, $CDCl_3$) δ 199.49 (C2′ (CHO)), 170.83 (CH_3CO), 138.29, 137.67 and 137.65 (Cq Ar), 128.66, 128.64, 128.61, 128.20, 128.18, 128.14, 127.99 and 127.94 (C Ar), 81.90 (C2), 78.88 (C3), 77.30 (C4), 75.54 (CH_2Ph), 75.07 (CH_2Ph), 73.67 (CH_2Ph), 70.95 (C5), 69.58 (C1), 63.20 (C6), 41.26 (C1′) and 20.95 (CH_3CO).

MS: m/z = 519.6 $[M+H]^+$.

2.2.4. 2-(2,3,4-Tri-O-benzyl-6-acetyl-α-D-glucopyranosyl)-ethanol **10**

Compound **9** (2800 mg, 5.39 mmol) was dissolved in dry MeOH under argon. The solution was then cooled to 0 °C and $NaBH_4$ (2.16 mmol) was added in three portions. The reaction was stirred at 0 °C and followed by TLC (Hexane/EtOAc 6:4). After 4 h, glacial acetic acid was added at 0 °C until pH = 3. The reaction was concentrated, and the residue was diluted in dichloromethane, then washed with a HCl 1 N solution (1×) and twice with brine (2×). The organic phase was dried over Na_2SO_4, filtered and evaporated. The crude was purified by flash chromatography (silica gel, eluent: Hexane/EtOAc 5.5:4.5 + 1% MeOH), yielding compound **10** (2672 mg, 5.14 mmol, 95% yield).

^{1}H NMR (400 MHz, $CDCl_3$) δ 7.40–7.26 (m, 15H, m, CH Ar), 4.95 (d, J = 10.9 Hz, 1H, CH_2Ph), 4.88 (d, J = 10.9 Hz, 1H, CH_2Ph), 4.81 (d, J = 10.9 Hz, 1H, CH_2Ph), 4.73 (d, J = 11.6 Hz, 1H, CH_2Ph), 4.64 (d, J = 11.6 Hz, 1H, CH_2Ph), 4.59 (d, J = 10.9 Hz, 1H, CH_2Ph), 4.29 (dd, J = 11.7, 2.0 Hz, 1H, H6a), 4.26–4.14 (m, 2H, H1, H2), 3.87–3.75 (m, 4H, H2′a,b, H3, H5), 3.72 (dd, J = 9.2, 5.8 Hz, 1H, H6b), 3.43 (t, J = 9.0 Hz, 1H, H4), 2.44 (s, 1H, O*H*), 2.10–1.98 (m, 4H, CH_3CO, H1′a) and 1.98–1.86 (m, 1H, H1′b).

^{13}C NMR (101 MHz, $CDCl_3$) δ 170.86 (CH_3CO), 138.41, 137.92 and 137.74 (Cq Ar), 128.59, 128.57, 128.55, 128.13, 128.06, 128.03, 128.00, 127.98 and 127.85 (C Ar), 81.87 (C2), 79.46 (C3), 77.82 (C4), 75.49 (CH_2Ph), 75.00 (CH_2Ph), 73.37 (C5), 73.33 (CH_2Ph), 70.30 (C1), 63.77 (C6), 60.81 (C2′), 27.88 (C1′) and 20.91 (CH_3CO).

MS: m/z = 521.4 $[M+H]^+$, 543.5 $[M+Na]^+$.

2.2.5. 2-(2,3,4-Tri-O-benzyl-6-acetyl-α-D-glucopyranosyl)-1-azidoethane **11**

Alcohol **10** (2598 mg, 5 mmol) was dissolved in dry THF under argon. Ph_3P (15 mmol) was added and the solution cooled to 0 °C. Diisopropyl azodicarboxylate (DIAD, 15 mmol) and, after 10 min, diphenylphosphoryl azide ($(PhO)_2PON_3$, 16 mmol) were added dropwise; the reaction was then raised and stirred at room temperature. The disappearance of the starting compound was followed by TLC (Hexane/EtOAc 7:3); after 2 h, the crude was concentrated and purified by flash chromatography (silica gel, eluent: Hexane/EtOAc 9:1). A total of 2446 mg (4,48 mmol, 90% yield) of azide **11** was obtained.

^{1}H NMR (400 MHz, $CDCl_3$) δ 7.38–7.26 (m, 15H, CH Ar), 4.94 (d, J = 10.9 Hz, 1H, CH_2Ph), 4.86 (d, J = 10.8 Hz, 1H, CH_2Ph), 4.80 (d, J = 10.8 Hz, 1H, CH_2Ph), 4.71 (d, J = 11.6 Hz, 1H, CH_2Ph), 4.62 (d, J = 11.6 Hz, 1H, CH_2Ph), 4.56 (d, J = 10.9 Hz, 1H, CH_2Ph), 4.23 (d, J = 3.4 Hz, 2H, H6a,b), 4.16–4.07 (m, 1H, H1), 3.82–3.70 (m, 2H, H2, H3), 3.68–3.60 (m, 1H, H5), 3.50–3.27 (m, 3H, H4, H2′a,b), 2.05 (s, 3H, CH_3CO) and 1.96 (dd, J = 13.7, 6.5 Hz, 2H, H1′a,b).

^{13}C NMR (101 MHz, $CDCl_3$) δ 170.90 (CH_3CO), 138.45, 137.95 and 137.76 (Cq Ar), 128.66, 128.61, 128.23, 128.13, 128.06 and 127.92 (C Ar), 82.07 (C3), 79.48 (C2), 77.71 (C4), 75.60 (CH_2Ph), 75.17 (CH_2Ph), 73.38 (CH_2Ph), 71.34 (C1), 70.19 (C5), 63.64 (C6), 47.96 (C2′), 24.64 (C1′) and 21.93 (CH_3CO).

MS: m/z 546.5 = $[M+H]^+$.

2.2.6. 2-(2,3,4-Tri-O-benzyl-α-D-glucopyranosyl)-1-azidoethane **12**

Pure azido derivative **11** (2420 mg, 4.44 mmol) was dissolved in MeOH (25 mL, ≈0.2 M) and 2 mL of a methanolic solution of sodium methoxide (2.2 M) was added. The reaction was stirred at room temperature for 12 h. After the disappearance of the starting compound, checked by TLC (Hexane/EtOAc 7:3), an amount of acidic resin (Amberlite

IRA-120 H^+) was added to the reaction. The resin was filtered off and the solution was evaporated to dryness, affording compound **12** (2116 mg, 4.21 mmol, 95% yield), which did not require further purification.

^{1}H NMR (400 MHz, $CDCl_3$) δ 7.41–7.27 (m, 15H, CH Ar), 4.94 (d, J = 10.9 Hz, 1H, CH_2Ph), 4.88 (d, J = 10.9 Hz, 1H, CH_2Ph), 4.82 (d, J = 10.9 Hz, 1H, CH_2Ph), 4.72 (d, J = 11.6 Hz, 1H, CH_2Ph), 4.67–4.60 (m, 2H, CH_2Ph), 4.11 (dd, J = 13.2, 7.2 Hz, 1H, H1), 3.83–3.74 (m, 2H, H6a, H3), 3.74–3.64 (m, 2H, H2, H6b), 3.56–3.45 (m, 2H, H4, H5), 3.45–3.37 (m, 1H, H2′a), 3.37–3.27 (m, 1H, H2′b), 1.98 (dd, J = 13.8, 7.0 Hz, 2H, H1′a,b) and 1.87 (s, 1H, O*H*).

^{13}C NMR (101 MHz, $CDCl_3$) δ 138.60, 138.05, 138.02 (Cq Ar), 128.65, 128.57, 128.17, 128.09, 128.04, 128.01 and 127.84 (C Ar), 82.11 (C3), 79.69 (C2), 77.85 (C4), 75.55 (*C*H_2Ph), 75.22 (*C*H_2Ph), 73.44 (*C*H_2Ph), 72.14 (C5), 71.38 (C1), 62.34 (C6), 48.04 (C2′) and 24.71 (C1′).

MS: m/z = 504.4 $[M+H]^+$, 526.3 $[M+Na]^+$.

2.2.7. 2-(2-(2-(Pent-4-en-1-yloxy)ethoxy)ethoxy)ethan-1-ol **13**

Compound **13** was prepared according to a procedure described in [62].

A solution of 1006 mL of NaOH 50% (12.6 mmol) was added to 10 g of triethyleneglycol at 100 °C. The reaction was stirred for 30 min at 100 °C and 5-bromo-1-pentene (12.6 mmol) was added and the reaction stirred at the same temperature for 24 h. The reaction was followed by TLC (CH_2Cl_2/MeOH 9:1). After 24 h, the reaction was diluted with water and extracted six times with EtOAc. The organic phases were combined, dried over Na_2SO_4 and evaporated; the crude was purified by flash chromatography (silica gel, eluent CH_2Cl_2/MeOH 11:1). A total of 2039 g (9.34 mmol, 74% yield) of monopentenylated triethylenglycol **13** was obtained.

^{1}H NMR (400 MHz, $CDCl_3$) δ 5.75 (ddt, J = 16.9, 10.1, 6.6 Hz, 1H, H4), 4.96 (dd, J = 17.2, 1.6 Hz, 1H, H5a), 4.90 (d, J = 10.2 Hz, 1H, H5b), 4.08 (t, J = 5.1 Hz, 1H, O*H*), 3.66 (d, J = 3.7 Hz, 2H, -CH_2CH_2O), 3.63–3.57 (m, 6H, -CH_2CH_2O), 3.57–3.50 (m, 4H, -CH_2CH_2O), 3.42 (t, J = 6.7 Hz, 2H, H1a,b), 2.05 (q, J = 7.3 Hz, 2H, H3a,b) and 1.68–1.57 (m, 2H, H2a,b).

^{13}C NMR (101 MHz, $CDCl_3$) δ 138.15 (C4), 114.84 (C5), 72.73, 70.80, 70.53, 70.44, 70.12 and 69.94 (-CH_2CH_2O), 61.49 (C1), 30.15 (C3) and 28.61 (C2).

MS: m/z = 219.2 $[M+H]^+$.

2.2.8. 2-(2-(2-(Pent-4-en-1-yloxy)ethoxy)ethoxy)ethyl-4-methylbenzenesulfonate **14**

To a solution of compound **13** (1.62 g, 7421 mmol) and DMAP (0.148 mmol) in CH_2Cl_2 (40 mL, ≈0.2 M), *p*-toluenesulphonyl chloride (14.84 mmol) and Et_3N (18.55 mmol) were added. The reaction was stirred at r.t. and followed by TLC (CH_2Cl_2/MeOH 9.5:0.5). After 10 h, TLC indicated the disappearance of the starting material, and 40 mL of water was added. The organic phase was separated and the aqueous phase was extracted thrice with CH_2Cl_2. The combined organic phases were dried with Na_2SO_4 and evaporated. The crude was purified by flash chromatography (silica gel, eluent CH_2Cl_2/MeOH 9.9:0.1), affording tosylate **14** (1976 g, 5.3 mmol, 72% yield).

^{1}H NMR (400 MHz, $CDCl_3$) δ 7.79 (d, J = 8.2 Hz, 2H, CH Ar), 7.33 (d, J = 8.0 Hz, 2H, C*H* Ar), 5.80 (ddt, J = 16.8, 10.1, 6.6 Hz, 1H, H4), 5.00 (dd, J = 17.1, 1.5 Hz, 1H, H5a), 4.94 (d, J = 9.4 Hz, 1H, H5b), 4.20–4.09 (m, 2H, -CH_2CH_2OTs), 3.72–3.64 (m, 2H, CH_2CH_2OTs), 3.64–3.52 (m, 8H, -CH_2CH_2O-), 3.45 (t, J = 6.7 Hz, 2H, H1a,b), 2.44 (s, 3H, CH_3PhSO$_3$), 2.10 (q, J = 7.2 Hz, 2H, H3a,b) and 1.72–1.60 (m, 2H, H2a,b).

^{13}C NMR (101 MHz, $CDCl_3$) δ 144.90 (Cq Ar), 138.36 (C4), 133.04 (Cq Ar), 129.92 and 128.08 (C Ar), 114.82 (C5), 70.86, 70.81, 70.74, 70.64, 70.17, 69.36 and 68.77 (CH_2CH_2O-), 30.32 (C3), 28.84 (C2) and 21.77 (*C*H_3PhSO$_3$).

MS: m/z = 373.4 $[M+H]^+$.

2.2.9. 2-(2,3,4-Tri-O-benzyl-6-(2-(2-(2-(pent-4-en-1-yloxy)ethoxy)ethoxy)ethyl)-α-D-glucopyranosyl)-1-azidoethane **15**

Compound **12** (1024 mg, 2036 mmol) was dissolved in dry DMF (20 mL, 0.1 M) under argon and 3054 mmol of NaH (60% dispersion in mineral oil) was added at room temperature; after 10 min, a solution of tosylate **14** (3.9 mmol) in 5 mL of dry DMF was added dropwise. The reaction was stirred at r.t. under argon atmosphere and followed by TLC (Hexane/EtOAc 7:3). After 12 h, the reaction was quenched by adding some drops of MeOH; the mixture was diluted with water and extracted three times with EtOAc. The organic phase was dried over sodium sulfate, filtered and evaporated and the crude purified by flash chromatography (silica gel, eluent Hexane/EtOAc 7:3), affording 1065 g (1.7 mmol, 83% yield) of compound **15**.

^{1}H NMR (400 MHz, $CDCl_3$) δ 7.35–7.22 (m, 15H, CH Ar), 5.79 (ddt, J = 16.9, 10.1, 6.6 Hz, 1H, H10), 4.99 (dd, J = 17.1, 1.6 Hz, 1H, H11a), 4.93 (d, J = 12.0 Hz, 1H, H11b), 4.90 (d, J = 11.1 Hz, 1H, C*H*$_2$Ph), 4.84 (d, J = 10.9 Hz, 1H, C*H*$_2$Ph), 4.79 (d, J = 10.9 Hz, 1H, C*H*$_2$Ph), 4.69 (d, J = 11.6 Hz, 1H, C*H*$_2$Ph), 4.63 (d, J = 11.0 Hz, 1H, C*H*$_2$Ph), 4.59 (d, J = 11.6 Hz, 1H, C*H*$_2$Ph), 4.15–4.05 (m, 1H, H1), 3.75–3.70 (m, 2H, H2, H3), 3.68–3.54 (m, 13H, H4, -C*H*$_2$C*H*$_2$O-), 3.54–3.47 (m, 3H, H5, H6a,b), 3.42 (t, J = 6.7 Hz, 2H, H7a,b), 3.39–3.25 (m, 2H, H2′a,b), 2.08 (dd, J = 14.2, 7.3 Hz, 2H, H9a,b), 1.99–1.89 (m, 2H, H1′a,b) and 1.70–1.60 (m, 2H, H8a,b).

^{13}C NMR (101 MHz, $CDCl_3$) δ 138.70 (Cq Ar), 138.39 (C10), 138.34 (Cq Ar), 138.09 (Cq Ar), 128.58, 128.55, 128.50, 128.04, 128.01, 127.98, 127.88 and 127.74 (C Ar), 114.80 (C11), 82.31 (C3), 79.63 (C2), 77.98 (C4), 75.59 (*C*H$_2$Ph), 75.16 (*C*H$_2$Ph), 73.37 (*C*H$_2$Ph), 71.67 (C1), 71.43 (C5), 71.10, 70.78, 70.73, 70.67, 70.59, 70.29 and 70.15 (C6, *C*H$_2$*C*H$_2$O-), 48.02 (C2′), 30.32 (C9), 28.84 (C8) and 24.47 (C1′).

MS: m/z = 704.7 $[M+H]^+$.

2.2.10. 2-(2,3,4-Tri-O-benzyl-6-(1-thioacetylpentyl-(5-(2-(2-(2-hydroxyethoxy)ethoxy) ethyl)))-α-D-glucopyranosyl)-1-azidoethane **16**

Compound **15** (384 mg, 0.545 mmol) was dissolved in CH_2Cl_2 (5.4 mL, 0.1 M) and the solution transferred into a sealed glass vial; thioacetic acid (0.656 mmol) and DPAP (0.055 mmol) were added and the reaction was stirred at r.t. under UV light exposure at 365 nm (using a UVA lamp of 4 W located 2 cm away from the glass vial). The progress of the reaction was followed by TLC (Hexane/EtOAc 7:3). After 2 h, TLC indicated the disappearance of the starting material; the crude was directly subjected to flash chromatography (silica gel, eluent Hexane/EtOAc 7:3), which afforded pure thioester **16** (357 mg, 0.46 mmol, 85% yield).

^{1}H NMR (400 MHz, $CDCl_3$) δ 7.36–7.27 (m, 15H, CH Ar), 4.91 (d, J = 10.9 Hz, 1H, C*H*$_2$Ph), 4.85 (d, J = 10.9 Hz, 1H, C*H*$_2$Ph), 4.81 (d, J = 10.9 Hz, 1H, C*H*$_2$Ph), 4.70 (d, J = 11.6 Hz, 1H, C*H*$_2$Ph), 4.67–4.58 (m, 2H, C*H*$_2$Ph), 4.16–4.07 (m, 1H, H1), 3.75–3.71 (m, 2H, H2, H3), 3.69–3.47 (m, 16H, H4, H5, H6a,b, C*H*$_2$C*H*$_2$O-), 3.44–3.27 (m, 4H, H7a,b, H2′a,b), 2.85 (t, J = 7.3 Hz, 2H, H11a,b), 2.31 (s, 3H, C*H*$_3$C(O)S), 2.00–1.90 (m, 2H, H1′a,b), 1.62–1.52 (m, 4H, H10a,b, H8a,b) and 1.46–1.34 (m, 2H, H9a,b).

^{13}C NMR (101 MHz, $CDCl_3$) δ 196.10 (CH$_3$*C*(O)S), 138.73, 138.37 and 138.12 (Cq Ar), 128.61, 128.58, 128.52, 128.07, 128.03, 128.01, 127.91 and 127.76 (C Ar), 82.34 (C3), 79.67 (C2), 78.02 (C4), 75.61 (*C*H$_2$Ph), 75.19 (*C*H$_2$Ph), 73.40 (*C*H$_2$Ph), 71.71 (C1), 71.46 (C5), 71.22, 71.12, 70.75, 70.70, 70.61, 70.34 and 70.18 (C6 sugar, *C*H$_2$*C*H$_2$O-), 48.06 (C2′), 30.79 (*C*H$_3$C(O)S), 29.49 (C8), 29.23 (C10), 29.16 (C11), 25.49 (C9) and 24.51 (C1′).

MS: m/z = 780.6 $[M+H]^+$, 752.6 $[M-N_2+H]^+$, 802.6 $[M+Na]^+$, 818.6 $[M+K]^+$.

2.2.11. 2-(2,3,4-Tri-O-benzyl-6-(1-thio-(5-(2-(2-(2-hydroxyethoxy)ethoxy)ethyl)))-α-D-glucopyranosyl)-1-azidoethane (dimer) **17**

Pure thioester **16** (38 mg, 0.049 mmol) was dissolved in MeOH (1 mL, 0.05 M) and 1.3 mg (0.024 mmol) of solid sodium methylate was added. The reaction was stirred at r.t. whilst exposed to air to promote the oxidation of the thiol group into a disulfide bond. After 24 h, TLC (Hexane/EtOAc 6.5:3.5) indicated the completion of the reaction. The reaction

mixture was concentrated to dryness; ^{1}H-NMR analysis of the crude sample indicated the complete removal of the acetyl group and the formation of a disulfide bond (triplet signal at 2.65 ppm). The residue was re-suspended in CH_2Cl_2, and the undissolved material was filtered off and discarded; the filtrate was concentrated to dryness and directly used for the next reaction.

^{1}H NMR (crude sample) (500 MHz, $CDCl_3$) δ 7.37–7.24 (m, 15H, CH Ar), 4.94–4.90 (m, 1H, CH_2Ph), 4.85 (d, J = 10.9 Hz, 1H, CH_2Ph), 4.81 (d, J = 10.9 Hz, 1H, CH_2Ph), 4.72–4.68 (m, 1H, CH_2Ph), 4.65–4.59 (m, 2H, CH_2Ph), 4.12 (dt, J = 9.8, 5.0 Hz, 1H, H1), 3.73 (dd, J = 8.5, 6.0 Hz, 2H, H2, H3), 3.70–3.49 (m, 16H, CH_2CH$_2$O-, H4, H5, H6a,b), 3.44–3.29 (m, 4H, H7a,b, H2′a,b), 2.71–2.62 (t, 2H, J = 7.3 Hz, H11a,b), 2.01–1.89 (m, 2H, H1′a,b), 1.68 (dt, J = 15.0, 7.5 Hz, 2H, H10a,b), 1.62–1.52 (m, 2H, H8a,b) and 1.47–1.37 (m, 2H, H9a,b).

2.2.12. 2-(6-(1-Thio-(5-(2-(2-(2-hydroxyethoxy)ethoxy)ethyl)))-α-D-glucopyranosyl)-1-aminoethane (dimer) **18**

Compound **18** was prepared following a Birch reduction protocol on protected derivative **17**, according to a procedure described in [63], with slight modifications. Some drops of liquid ammonia were collected in a two-necked round-bottomed flask cooled to −78 °C and a small piece of sodium (approx. 20–30 mg) was added. The solution turned blue immediately, and after 10 min, a dry THF solution (1,4 mL) of the crude compound **17** was added. The reaction was stirred at −78 °C for 15 min, then powdered NH_4Cl (≈200 mg) was added and the reaction was warmed to r.t. The solvent was evaporated and the crude was subjected to reverse phase C18 chromatography (gradient eluent: H_2O–MeOH); a total of 14 mg (0.032 mmol as monomer, 65% yield over two steps) of **18** was obtained.

^{1}H NMR (500 MHz, CD_3OD) δ 4.11 (ddd, J = 11.6, 5.1, 2.7 Hz, 1H, H1), 3.79–3.58 (m, 18H, H2, H3, H4, H5, H6a,b, CH_2CH$_2$O-), 3.51 (t, J = 6.6 Hz, 2H, H7a,b), 3.23–3.18 (m, 1H, H2′a), 3.17–3.10 (m, 1H, H2′b), 2.74–2.67 (m, 2H, H11a,b), 2.15–2.05 (m, 1H, H1′a), 1.99–1.90 (m, 1H, H1′b), 1.76–1.68 (m, 2H, H10a,b), 1.66–1.57 (m, 2H, H8a,b) and 1.51–1.43 (m, 2H, H9a,b).

^{13}C NMR (101 MHz, CD_3OD) δ 76.10 (C1), 74.44, 71.87, 71.23, 70.73, 70.63, 70.60, 70.32 and 70.17 (C3, C2, C4, C5, C6, C7, CH_2CH$_2$O- × 6), 39.63 (C11), 38.06 (C2′), 29.45 (C8), 29.21 (C10), 25.63 (C9) and 24.20 (C1′).

MS: m/z = 882.2 $[M+H]^+$.

2.2.13. 5-(N,N-Dimethylamino)-N-(2-(6-(1-thio-(5-(2-(2-(2-hydroxyethoxy)ethoxy)ethyl)))-α-D-glucopyranosyl)-naphthalene-1-sulfonamide (dimer) **2**

Compound **18** (10 mg, 0.023 mmol as monomer) was dissolved in MeOH; Et_3N (10 µL) and dansyl chloride (16 mg, 0.06 mmol) were added and the reaction was stirred at r.t. The reaction was followed by TLC (EtOAc/MeOH 9:1 and EtOAc/MeOH/H_2O/AcOH 5:5:1:1). After 10 h, the crude was purified by normal phase flash chromatography (silica gel, eluent: EtOAc/MeOH 8:2) and then with reverse phase C18 Cartridge, affording 6 mg (0.009 mmol, 39% yield) of compound **2**.

^{1}H NMR (500 MHz, CD_3OD) δ 8.54 (t, J = 14.1 Hz, 1H, CH Ar), 8.36 (d, J = 8.7 Hz, 1H, CH Ar), 8.21 (dd, J = 7.3, 1.1 Hz, 1H, CH Ar), 7.59 (t, J = 7.7 Hz, 2H, CH Ar), 7.27 (d, J = 7.3 Hz, 1H, CH Ar), 3.86–3.77 (m, 1H, H1), 3.68–3.63 (m, 2H, H6a, CH_2CH$_2$O-), 3.62–3.55 (m, 10H, CH_2CH$_2$O-), 3.55–3.51 (m, 2H, H6b, CH_2CH$_2$O-), 3.49–3.42 (m, 3H, H2, H7a,b), 3.39–3.34 (m, 2H, H3, H5), 3.18–3.11 (m, 1H, H4), 3.00–2.91 (m, 2H, H2′a,b), 2.88 (s, 6H, (CH_3)$_2$N-), 2.65 (t, J = 7.2 Hz, 2H, H11a,b), 1.77–1.71 (m, 2H, H1′a,b), 1.69–1.62 (m, 2H, H10a,b), 1.60–1.51 (m, 2H, H8a,b) and 1.47–1.39 (m, 4H, H9a,b).

^{13}C NMR (101 MHz, CD_3OD) δ 152.4 (CqAr), 135.2 (CqAr), 131.18 (CH Ar), 130.9 (CqAr), 130.32 (CH Ar), 129.12 (CH Ar), 124.39 (CH Ar), 120.60 (CH Ar), 116.43 (CH Ar), 114.2 (CqAr), 75.23, 75.05, 73.52, 72.56 and 72.17 (C1, C2, C3, C4, C5), 72.93, 72.13, 71.92, 71.52, 71.50 and 71.30 (C7, CH_2CH$_2$O- x 6), 57.46 (C6), 45.85 (CH_3)$_2$N-), 39.82 (C11), 41.30 (C2′), 29.78 (C8), 29.45 (C10), 26.12 (C1′) and 25.23 (C9).

MS: m/z = 1348.8 $[M+H]^+$, 1370.7 $[M+Na]^+$.

2.3. Synthesis of L-Glutamine Derivative **4** and **5**

2.3.1. 5-(2-(2-(2-Azidoethoxy)ethoxy)ethoxy)pent-1-ene **19**

To a solution of tosylate **14** (1976 mg, 5.3 mmol) in dry DMF (35 mL), 15.9 mmol of NaN_3 was added. The reaction was stirred at r.t. for 2 h and then at 80 °C for 10 h. The reaction was followed by TLC (Hexane/EtOAc 8:2). At the end of the reaction, the suspension was diluted with water and extracted with EtOAc (3×). The organic phases were combined, dried over sodium sulphate and evaporated. The residue was purified by flash chromatography (silica gel, eluent: Hexane/EtOAc 8:2), affording azide **19** (1012 mg, 4.16 mmol, 78% yield).

^{1}H NMR (400 MHz, $CDCl_3$) δ 5.80 (ddt, J = 16.9, 10.2, 6.7 Hz, 1H, H4), 5.01 (dd, J = 17.1, 1.6 Hz, 1H, H5a), 4.95 (d, J = 10.2 Hz, 1H, H5b), 3.72–3.61 (m, 8H, -OCH_2CH_2-), 3.61–3.54 (m, 2H, -OCH_2CH_2-), 3.46 (t, J = 6.7 Hz, 2H, H1a,b), 3.38 (t, J = 5.0 Hz, 2H, -OCH$_2$CH_2N$_3$), 2.10 (q, J = 7.3 Hz, 2H, H3a,b) and 1.73–1.61 (m, 2H, H2a,b).

^{13}C NMR (101 MHz, $CDCl_3$) δ 138.40 (C4), 114.80 (C5), 70.82, 70.81, 70.77, 70.21 and 70.15 (-OCH$_2$CH$_2$-), 50.78 (-OCH$_2$CH$_2$N$_3$), 30.34 (C3) and 28.86 (C2).

MS: m/z = 244.2 $[M+H]^+$.

2.3.2. 2-(2-(2-(Pent-4-en-1-yloxy)ethoxy)ethoxy)ethan-1-amine **20**

Compound **19** (1153 mg, 4.73 mmol) was dissolved in THF (30 mL) and Ph_3P (5.68 mmol) was added. The reaction was stirred at r.t. for 2 h, then 5.67 mmol of distilled water was added and the reaction was heated to 60 °C and stirred for 30 min, following the disappearance of the starting material observed by TLC (Hexane/EtOAc 8:2 and CH_2Cl_2/MeOH 9:1). The solvent was then evaporated and the crude purified by flash chromatography (silica gel, eluent: CH_2Cl_2/MeOH 9:1 to CH_2Cl_2/MeOH/NH_3 (aq) 7:3:1), affording amine **20** (0.951 g, 4.4 mmol, 93% yield).

^{1}H NMR (400 MHz, CD_3OD) δ 5.83 (ddt, J = 13.5, 10.1, 6.7 Hz, 1H, H4), 5.02 (dd, J = 17.1, 1.1 Hz, 1H, H5a), 4.95 (d, J = 10.1 Hz, 1H, H5b), 3.69–3.53 (m, 12H, -OCH_2CH_2-), 3.52–3.45 (m, 2H, -OCH$_2$CH_2NH$_2$), 2.12 (dd, J = 14.4, 7.2 Hz, 2H, H3a,b) and 1.72–1.58 (m, 2H, H2a,b).

^{13}C NMR (101 MHz, CD_3OD) δ 139.44 (C4), 115.23 (C5), 73.67, 71.56, 71.50, 71.26, 71.12 and 70.39 (C1, -OCH$_2$CH$_2$-), 41.42 (-OCH$_2$CH$_2$NH$_2$), 31.33 (C3) and 30.03 (C2).

MS: m/z = 218.3 $[M+H]^+$.

2.3.3. (9H-Fluoren-9-yl)methyl-(S)-(3,7-dioxo-1,1,1-triphenyl-11,14,17-trioxa-2,8-diazadocos-21-en-6-yl) carbamate **21**

Compound **20** (133 mg, 0.612 mmol) was dissolved in dry CH_2Cl_2 (6 mL, 0.1 M) in argon atmosphere. The solution was cooled to 0 °C and Fmoc-L-Gln(Trt)-OH (0.64 mmol), HOBt (0.918 mmol) and EDC (0.918 mmol) were added. The reaction was warmed to r.t. and stirred under argon. After 15 h, TLC (CH_2Cl_2/MeOH 9.5:0.5 and CH_2Cl_2/MeOH/NH_3 (aq) 9:1:0.1) indicated the absence of the starting compound; the reaction was diluted with CH_2Cl_2 and washed with water (3×). The organic phase was collected, dried over sodium sulphate, filtered and evaporated. The crude was purified by flash chromatography on Biotage System (silica gel, gradient CH_2Cl_2 100%–CH_2Cl_2/MeOH 9.3:0.7). A total of 390 mg (0.48 mmol) of compound **21** was obtained (79% yield).

^{1}H NMR (500 MHz, $CDCl_3$) δ 7.80 (d, J = 7.5 Hz, 2H, CH Ar Fmoc), 7.63 (d, J = 7.4 Hz, 2H CH Ar Fmoc), 7.43 (t, J = 7.4 Hz, 2H CH Ar Fmoc), 7.38–7.20 (m, 17H, CH Ar Fmoc, CH Ar Trt), 7.11 (s, 1H, CON*H*Trt), 6.84 (s, 1H, -N*H*CH$_2$CH$_2$O-), 6.04 (d, J = 6.7 Hz, 1H, CON*H* Fmoc), 5.83 (ddt, J = 16.9, 10.2, 6.6 Hz, 1H, H15), 5.04 (ddd, J = 17.1, 3.3, 1.5 Hz, 1H, H16a), 5.01–4.96 (m, 1H, H16b), 4.41 (d, J = 7.1 Hz, 2H, NHCOCH_2-Fmoc), 4.24 (t, J = 7.0 Hz, 1H, C*H* Fmoc), 4.19–4.10 (m, 1H, H4), 3.64–3.51 (m, 10H, H7, H8, H9, H10, H11), 3.49–3.40 (m, 4H, H12a,b, H6a,b), 2.58–2.49 (m, 1H, H2a), 2.49–2.39 (m, 1H, H2b), 2.18–2.07 (m, 3H, H14a,b, H3a), 2.03–1.95 (m, 1H, H3b) and 1.73–1.65 (m, 2H, H13a,b).

^{13}C NMR (101 MHz, $CDCl_3$) δ 171.80 (C5), 171.32 (C1), 156.23 (OCONH Fmoc), 144.48 (Cq Ar Trt), 143.80 (Cq Ar Fmoc), 143.68 (Cq Ar Fmoc), 141.17 (Cq Ar Fmoc), 141.14 (Cq

Ar Fmoc), 138.11 (C15), 128.64 (C Ar Trt, C Ar Fmoc), 127.82 (C Ar Trt, C Ar Fmoc), 127.62 (C Ar Trt, C Ar Fmoc), 127.01 (C Ar Trt, C Ar Fmoc), 126.88 (C Ar Trt, C Ar Fmoc), 125.10 (C Ar Fmoc), 119.87 (C Ar Fmoc), 114.73 (C16), 70.56, 70.48, 70.37, 70.34, 70.07 and 69.90 (C7, C8, C9, C10, C11, Cq Trt), 69.30 (C12), 66.76 (NHCOCH_2-Fmoc), 54.06 (C4), 47.06 (*C*H Fmoc), 39.20 (C6), 33.17 (C2), 30.11 (C14), 29.33 (C3) and 28.59 (C13).

MS: m/z = 810.9 $[M+H]^+$.

2.3.4. (S)-2-amino-N1-(2-(2-(2-(pent-4-en-1-yloxy)ethoxy)ethoxy)ethyl)pentanediamide **22**

Compound **21** (148 mg, 0.18 mmol) was dissolved in 1.8 mL of CH_2Cl_2 (0.1 M) and 0.4 mL of TFA was added. After 6 h, TLC (CH_2Cl_2/MeOH 9.5:0.5) showed no more starting compound (Trt deprotection) and the reaction was neutralized to pH 7 with NH_3(aq). The solvent was evaporated and the residue was dissolved in DMF (8 mL). Piperidine was added (2 mL) and the reaction was stirred at r.t. After 12 h, TLC showed the formation of a more polar compound (Fmoc removal); the reaction was then concentrated and the residue purified by flash chromatography (silica gel, eluent CH_2Cl_2/MeOH/NH_3 (aq) 8.5:1.5:0.1). A total of 60 mg (0.17 mmol) of deprotected compound **22** was obtained (96% yield).

^{1}H NMR (500 MHz, CD_3OD) δ 5.83 (ddt, J = 17.0, 10.2, 6.7 Hz, 1H, H15), 5.02 (ddd, J = 17.1, 3.5, 1.6 Hz, 1H, H16a), 4.95 (ddt, J = 10.2, 2.2, 1.2 Hz, 1H, H16b), 3.67–3.60 (m, 6H, -C$H_2$$CH_2O$-), 3.60–3.54 (m, 4H, -C$H_2$$CH_2O$-), 3.48 (t, J = 6.5 Hz, 2H, H12a,b), 3.46–3.33 (m, 3H, H4, H6a,b), 2.28 (t, J = 7.8 Hz, 2H, H2a,b), 2.15–2.09 (m, 2H, H14a,b), 1.99–1.90 (m, 1H, H3a), 1.88–1.79 (m, 1H, H3b) and 1.70–1.62 (m, 2H, H13a,b).

^{13}C NMR (101 MHz, CD_3OD) δ 173.20 (C5), 172.90 (C1), 138.78 (C15), 115.91 (C16), 70.65, 70.62, 70.38, 70.34, 70.12 and 69.85 (C7, C8, C9, C10, C11), 69.45 (C12), 54.06 (C4), 40.20 (C6), 32.17 (C2), 30.53 (C14), 29.26 (C3) and 28.87 (C13).

MS: m/z = 346.4 $[M+H]^+$, 368.4 $[M+Na]^+$.

2.3.5. (S)-S-(1,4-Diamino-1,5-dioxo-9,12,15-trioxa-6-azaicosan-20-yl)-ethanethioate **23**

Compound **22** (60 mg, 0.174 mmol) was dissolved in MeOH (1.7 mL, 0.1 M). Thioacetic acid (0.23 mmol) and DPAP (0.035 mmol) were added to this solution and the reaction was stirred at r.t. under UV light exposure at 365 nm. After 2 h, TLC (CH_2Cl_2/MeOH/NH_3 (aq) 7:3:0.2) indicated the complete conversion of the starting compound; the reaction was concentrated and the residue was purified by flash chromatography (silica gel, eluent CH_2Cl_2/MeOH/NH_3 (aq) 8.5:1.5:0.1). A total of 29 mg (0.07 mmol) of thioester **23** was obtained (47% yield).

^{1}H NMR (500 MHz, CD_3OD) δ 4.32 (dd, J = 8.4, 5.7 Hz, 1H, H4), 3.66–3.60 (m, 6H, -C$H_2$$CH_2O$-), 3.60–3.53 (m, 4H, -C$H_2$$CH_2O$-), 3.47 (t, J = 6.5 Hz, 2H, H12a,b), 3.40 (t, J = 5.4 Hz, 1H, H6a), 3.36 (t, J = 5.5 Hz, 1H, H6b), 2.87 (t, J = 7.3 Hz, 2H, H16a,b), 2.34–2.26 (m, 5H, CH_3COSCH_2, H2a,b), 2.11–2.01 (m, 1H, H3a), 1.95–1.86 (m, 1H, H3b), 1.63–1.55 (m, 4H, H13a,b, H15a,b) and 1.47–1.39 (m, 2H, H14a,b).

^{13}C NMR (101 MHz, CD_3OD) δ 197.53 (CH_3*C*(O)S-), 173.91 (C5), 173.30 (C1), 72.04, 71.62, 71.56, 71.28, 71.14 and 70.44 (-CH_2CH_2O-), 54.38 (C4), 40.39 (C6), 32.56 (C2), 30.62 (C13), 30.52 (*C*H_3C(O)S-), 30.17 (C15), 29.77 (C16), 29.10 (C3) and 26.39 (C14).

MS: m/z = 422.6 $[M+H]^+$, 444.5 $[M+Na]^+$.

2.3.6. (S)-2-Amino-N1-(2-(2-(2-((5-mercaptopentyl)oxy)ethoxy)ethoxy)ethyl) pentanediamide (dimer) **4**

Compound **23** (10 mg, 0.0237 mmol) was dissolved in 0.6 mL of MeOH (previously degassed under a stream of argon) and 0.06 mmol of sodium methoxide was added. The reaction was stirred at r.t., and after 24 h, a sample of the crude was analyzed by ^{1}H-NMR to check the complete thioester deprotection. The spectrum clearly indicated the disappearance of the triplet at 2.9 ppm (-CH_2-SAc) and of the singlet at 2.3 ppm (CH_3C(O)S-). A new triplet at 2.65 ppm was present, indicating the formation of a disulfide bond. The reaction was then acidified with HCl 1 N (final pH = 6) and the solvent evaporated. The crude was directly used for the preparation of the nanoparticles.

^{1}H NMR (500 MHz, CD_3OD) δ 4.31 (dd, J = 8.6, 5.6 Hz, 1H, H4), 3.68–3.58 (m, 8H, -C*H*$_2$CH$_2$O-), 3.56 (t, J = 5.5 Hz, 2H, -CH$_2$C*H*$_2$O-), 3.49 (t, J = 6.5 Hz, 2H, H12a,b), 3.44–3.33 (m, 2H, H6a,b), 2.70 (t, J = 7.2 Hz, 2H, H16a,b), 2.30 (t, J = 7.6 Hz, 2H, H2a,b), 2.11–2.03 (m, 1H, H3a), 1.96–1.90 (m, 1H, 3b), 1.71 (dt, J = 14.7, 7.3 Hz, 2H, H15a,b), 1.65–1.56 (m, 2H, H13a,b) and 1.54–1.43 (m, 2H, H14a,b).

^{13}C NMR (101 MHz, $CDCl_3$) δ 174.01 (C5), 173.33 (C1), 72.13, 71.50, 71.47, 71.24, 71.08 and 70.55 (-CH$_2$CH$_2$O-), 54.49 (C4), 40.33 (C6), 39.54 (C16), 32.55 (C2), 30.26 (C13), 30.00 (C15), 29.01 (C3) and 26.03 (C14).

MS: m/z = 758.1 $[M+H]^+$.

2.3.7. Tert-butyl (S)-2-((tert-butoxycarbonyl)amino)-5-oxo-9,12,15-trioxa-6-azaicos-19-enoate **24**

Boc-L-glutamic acid 1-tert-butyl ester (149 mg, 0.49 mmol) and compound **20** (0.58 mmol) were dissolved in CH_2Cl_2 (4.9 mL, 0.1 M) under argon and 0.98 mmol of Et_3N was added; the solution was stirred at r.t. for 15 min. The temperature was set to 0 °C and HOBt (0.73 mmol) and DCC (0.73 mmol) were added. The reaction was stirred at r.t. until TLC (CH_2Cl_2/MeOH 9.5:0.5) indicated the disappearance of the starting material. The reaction was recovered as described for compound **22** and the product was purified by flash chromatography (silica gel, eluent CH_2Cl_2/MeOH 9.8:0.2), affording compound **24** (207 mg, 0.47 mmol, 95% yield).

^{1}H NMR (400 MHz, $CDCl_3$) δ 6.44 (s, 1H, -N*H*CH$_2$CH$_2$O-), 5.80 (td, J = 16.9, 6.7 Hz, 1H, H15), 5.26 (d, J = 7.6 Hz, 1H, N*H*Boc), 5.01 (d, J = 17.2 Hz, 1H, H16a), 4.95 (d, J = 10.2 Hz, 1H, H16b), 4.14 (s, 1H, H2), 3.67–3.52 (m, 10H, -C*H*$_2$CH$_2$O-), 3.51–3.36 (m, 4H, H12a,b, H6a,b), 2.30–2.20 (m, 2H, H4a,b), 2.18–2.00 (m, 3H, H14a,b, H3a), 1.95–1.81 (m, 1H, H3b), 1.74–1.62 (m, 2H, H13a,b) and 1.50–1.37 (m, 18H, $(CH_3)_3$ -Boc, -tBu).

^{13}C NMR (101 MHz, $CDCl_3$) δ 172.20 (C5), 171.57 (C1), 155.81 (OCONH Boc), 138.25 (C15), 114.87 (C16), 82.14 (Cq OtBu), 79.78 (Cq Boc), 70.77, 70.59, 70.33, 70.12 and 69.87 (C7-C12), 53.71 (C2), 39.37 (C6), 32.70 (C4), 30.27 (C14), 29.14 (C3), 28.78 (C13), and 28.40 and 28.05 ($(CH_3)_3$ OtBu, Boc).

MS: m/z = 503.4 $[M+H]^+$.

2.3.8. (S)-2-Amino-5-oxo-9,12,15-trioxa-6-azaicos-19-enoic acid **25**

Protected L-glutamine derivative **24** (246 mg, 0.49 mmol) was dissolved in a mixture of CH_2Cl_2/trifluoroacetic acid (12 mL/3 mL) and stirred at r.t. The reaction was followed by TLC (CH_2Cl_2/MeOH/NH_3 (aq) 7:3:0.3), and after 2 h, the solution was neutralized with NH_3 (aq). The crude was concentrated and the product purified by flash chromatography (silica gel, eluent: CH_2Cl_2/MeOH/NH_3 (aq) 7:3:0.2), yielding 52 mg (0.15 mmol, 30% yield) of compound **25**.

^{1}H NMR (400 MHz, CD_3OD) δ 5.83 (ddt, J = 17.0, 10.1, 6.8 Hz, 1H, H15), 5.07–4.96 (m, 2H, H16a,b), 3.67–3.52 (m, 11H, H2, H7a,b, H-8a,b, H9a,b, H10a,b, H11a,b), 3.49 (t, J = 6.5 Hz, 2H, H12a,b), 3.37 (t, J = 5.3 Hz, 2H, H6a,b), 2.46 (t, J = 7.1 Hz, 2H, H4a,b), 2.20–2.03 (m, 4H, H14a,b, H3a,b) and 1.72–1.62 (m, 2H, H13a,b).

^{13}C NMR (101 MHz, CD_3OD) δ 174.87 (C1), 173.28 (C5), 139.43 (C15), 115.24 (C16), 71.57, 71.51, 71.24, 71.08 and 70.47 (C7-C12), 55.10 (C2), 40.47 (C6), 32.91 (C4), 31.34 (C14), 29.98 (C13) and 27.79 (C3).

MS: m/z = 347.3 $[M+H]^+$.

2.3.9. (S)-22-Amino-2,19-dioxo-9,12,15-trioxa-3-thia-18-azatricosan-23-oic acid **26**

Compound **25** (50 mg, 0.144 mmol) was dissolved in MeOH (1.5 mL, 0.1 M). Thioacetic acid (0.19 mmol) and DPAP (0.03 mmol) were added to this solution and the reaction was stirred at r.t. under UV light exposure at 365 nm. After 2 h, TLC (CH_2Cl_2/MeOH/NH_3 (aq) 7:3:0.2) indicated the complete conversion of the starting compound; the reaction was concentrated and the residue was purified by flash chromatography (silica gel, eluent

CH_2Cl_2/MeOH/NH_3 (aq) 7:3:0.2). A total of 32 mg (0.075 mmol) of thioester **26** was obtained (53% yield).

^{1}H NMR (500 MHz, CD_3OD) δ 3.66–3.60 (m, 7H, -CH_2CH_2O-, H2), 3.60–3.57 (m, 2H, -CH_2CH_2O-), 3.55 (t, J = 5.4 Hz, 2H, H7), 3.48 (t, J = 6.5 Hz, 2H, H12), 3.37 (t, J = 5.5 Hz, 2H, H6), 2.87 (t, J = 7.3 Hz, 2H, H16a,b), 2.45 (t, J = 7.1 Hz, 2H, H4a,b), 2.30 (s, 3H, CH_3C(O)S), 2.18–2.04 (m, 2H, H3a,b), 1.64–1.55 (m, 4H, H15a,b, H13a,b) and 1.48–1.40 (m, 2H, H14a,b).

^{13}C NMR (101 MHz, CD_3OD) δ 197.51 (CH_3C(O)S), 190.57 and 175.09 (C1), 173.52 (C5), 72.02, 71.57, 71.52, 71.25, 71.09 and 70.50 (-CH_2CH_2O-), 55.63 (C2), 40.47 (C6), 33.07 (C4), 30.60 (C13), 30.53 (CH_3C(O)S), 30.14 (C15), 29.76 (C16), 27.97 (C3) and 26.36 (C14).

MS: m/z = 423.3 $[M+H]^+$.

2.4. General Procedure for the Preparation of Ligand-Loaded Gold Nanoparticles

The thiol-ending ligand (3 eq. overall) was dissolved in MeOH at a final concentration of 12 mM. For nanoparticles decorated with different ligands, a suitable methanolic mixture was prepared, with a total final concentration of the ligands set to 12 mM (3 eq. overall). To this solution, 1 eq of a 25 mM aqueous solution of $HAuCl_4$ (hydrogen tetrachloroaurate) was added. After the addition, the reaction was stirred for 5 min at room temperature. During this step, Au(I) polymers were formed, and the reaction became turbid, with a pale-yellow color. Then, a 1 M water solution of $NaBH_4$ (27–33 eq) was added in four portions, ensuring vigorous stirring during the addition. The formation of a black precipitate indicated the generation of Au nanoparticles. The reaction was left for 2 h at 25° C with 180 r.p.m. stirring. The black precipitate (AuNPs) was washed several times with MeOH, with three cycles of vortexing and centrifugation (12,000 rpm, 2 min), removing the supernatant and adding fresh MeOH. In this step, the excess of dissolved ligands, not attached to the NPs, was removed. The washed residue containing AuNPs was diluted in HPLC-grade water and then purified by dialysis (Spectrum™ Spectra/Por™ Float-A-Lyzer™, 10,000 MWCO, 1–5 mL volume). The water of the dialysis bath was replaced with fresh HPLC-grade water thrice per day for three days. The final water dispersion of the functionalized AuNPs was freeze-dried, obtaining a dark-black powder. The prepared AuNPs were stored at 4 °C and then subjected to ^{1}H NMR, UV–Vis spectroscopy and TEM analysis. The ratio between the thiol ligands attached to the AuNPs was assessed, recording ^{1}H-NMR spectra of the initial mixture and of the methanolic supernatants after AuNP formation.

2.4.1. Preparation of AuNP1

A solution of 4.97 mg of **GlcC$_5$SH** (17.6 μmol) in 1.47 mL of HPLC-grade MeOH, 234.7 μL of a 25 mM aqueous solution of HAuCl4 and 197 μL of a 1 M aqueous solution of $NaBH_4$ were used to obtain 1.21 mg of AuNP1.

2.4.2. Preparation of AuNP2

A 2.3:1 mixture solution of **GlcC$_5$SH** (1.954 mg, 6.92 μmol) and compound **2** (2 mg, 2.97 μmol) was mixed with 132 μL of a 25 mM aqueous solution of HAuCl4 and with 99 μL of a 1 M aqueous solution of $NaBH_4$, affording 1.12 mg of AuNP2.

2.4.3. Preparation of AuNP3

A 1:1 mixture solution of **GlcC$_5$SH** (0.75 mg, 2.642 μmol) and L-glutamine derivative **4** (1 mg, 2.642 μmol) was mixed with 70.5 μL of a 25 mM aqueous solution of HAuCl4 and with 58 μL of a 1 M aqueous solution of $NaBH_4$, affording 0.49 mg of AuNP3.

2.4.4. Preparation of AuNP4

A 1.4:1:1.6 mixture solution of **GlcC$_5$SH** (0.55 mg, 1.947 μmol), L-glutamine derivative **4** (0.526 mg, 1.391 μmol) and compound **2** (1.5 mg, 2.226 μmol) was mixed with 74.18 μL of a 25 mM aqueous solution of HAuCl4 and with 65 μL of a 1 M aqueous solution of $NaBH_4$, affording 0.23 mg of AuNP4.

A 1.4:1:1.6 mixture solution of **GlcC$_5$SH** (0.55 mg, 1.947 μmol), L-glutamine derivative **4** (0.526 mg, 1.391 μmol) and compound **2** (1.5 mg, 2.226 μmol) was mixed with 74.18 μL of a 25 mM aqueous solution of $HAuCl_4$ and with 65 μL of a 1 M aqueous solution of $NaBH_4$, affording 0.23 mg of AuNP4.

3. Results and Discussion

In the first phase of the present work, we designed a set of sulfur-functionalized derivatives of D-glucose, *C*-glucoside **1** and L-glutamine (Figure 3) in order to have the suitable compounds for the preparation of the corresponding gold nanoparticles (Figure 4) [54,64].

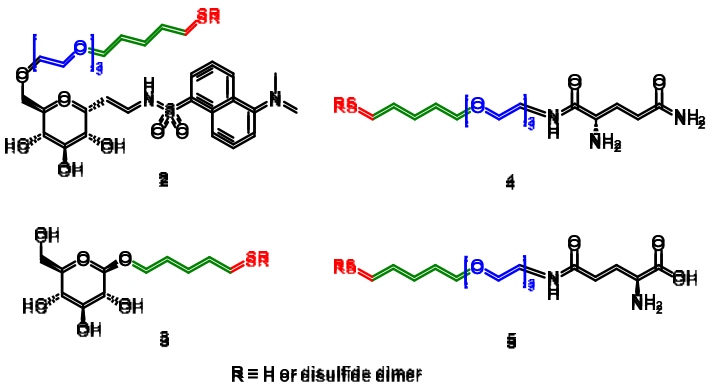

Figure 3. Sulfur-functionalized ligands for the preparation of the AuNPs.

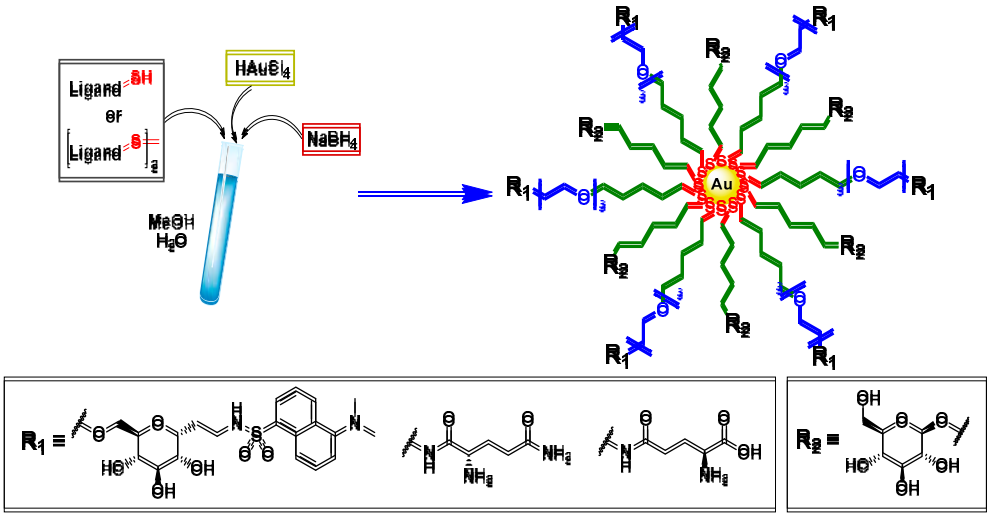

Figure 4. General structure of the designed nanoparticles: AuNPs decorated with the "active components" *C*-glucoside **2** and/or L-Gln **4** or **5**. The density of the "active components" can be modulated by varying their molar equivalents with respect to the "inner component" (**GlcC$_5$SH**).

The role of the D-glucose derivative *O*-(5′-thiopentyl)-β-D-glucopyranoside (compound **3**, **GlcC$_5$SH**), synthesized following a well-established protocol [65,66], was to improve the water dispersibility of the nanoparticles, since compound **1** showed low water solubility (approximately 0.5 mg/mL). Furthermore, **GlcC$_5$SH** was also selected as an "inner component" [51,66]. It should be noted that while ligands **2**, **4** and **5** have a long and amphiphilic linker to impart flexibility and assist in the water dispersibility of the final AuNPs, **GlcC$_5$SH** has a short and hydrophobic linker to ensure the rigidity of the nanoparticle and allow the above-mentioned ligands to protrude from the gold surface. **GlcC$_5$SH** should thus assist the multivalent effect of the other thiol-ending ligands, rather than interfering with their biological effects, since SGLT1-mediated anti-inflammatory effects are observed only with huge amounts of orally administered D-glucose.

Firstly, we designed the synthetic route of the derivatives considering the attachment of a suitable spacer/linker bearing a terminal thiol group. This linker ensured the correct spatial separation between the core of the gold nanoparticle and the "active component" (*C*-glucoside **1** or L-glutamine), which is necessary for the interaction of the bioactive molecules with the target receptor. The linker that we chose was composed

fects are observed only with huge amounts of orally administered D-glucose.

Firstly, we designed the synthetic route of the derivatives considering the attachment of a suitable spacer/linker bearing a terminal thiol group. This linker ensured the correct spatial separation between the core of the gold nanoparticle and the "active component" (*C*-glucoside **1** or L-glutamine), which is necessary for the interaction of the bioactive molecules with the target receptor. The linker that we chose was composed of a tri(ethyleneglycol) (TEG) chain and a five-carbon atom (C_5) spacer. Ethylene glycol polymers are extensively used in the pharmaceutical industry for their low toxicity, excellent solubility in aqueous media, resistance to non-specific protein adsorption and potential limited immunogenic and allergenic effects [67,68]. PEGylation is an important and emerging aspect in the drug delivery field; the conjugation of PEG to drugs has a positive impact on the pharmacokinetic and pharmacodynamic profile of the molecule to which it is conjugated. Moreover, polyethylene glycol (PEG) represents an inert polymer and is not metabolized. From a synthetic point of view, the insertion of a PEG chain on small molecules or drugs as well as biomacromolecules is now a relatively simple chemical transformation owing to numerous differently functionalized and commercially available PEG chains, and thanks to the development, over the last few decades, of many chemical (bio)orthogonal ligation strategies. For example, in a previous work, we developed a synthetic strategy to obtain heterobifunctionalized (poly)ethylene glycol chains for use as chemical tools in the modification of bioactive molecules and bio(macro)molecules [69]. The monofunctionalization of the triethyleneglycol linker with a pentenyl chain allowed for the introduction of a terminal double bond, which was exploited for the insertion of a sulfur-containing group through a thiol-ene coupling (TEC) reaction [70]. Several synthetic procedures allow for the conversion of a terminal alkene into a thioether linkage, for example, using a Michael addition reaction between a thiol compound and a α,β-unsaturated carbonyl compound or exploiting a radical mechanism, as in the case of AIBN-catalyzed reactions. We decided to use a radical photoinitiator, called 2,2-dimethoxy-2-phenylacetophenone (DPAP), which allows the reaction to occur in a faster and simpler fashion. This method permits the use of non-degassed solvents, and tolerates air atmosphere, moisture and even aqueous solvents. The reaction proceeded smoothly at room temperature; only a short (generally 30 min–1 h) UV light exposure at 365 nm was required (Scheme 1).

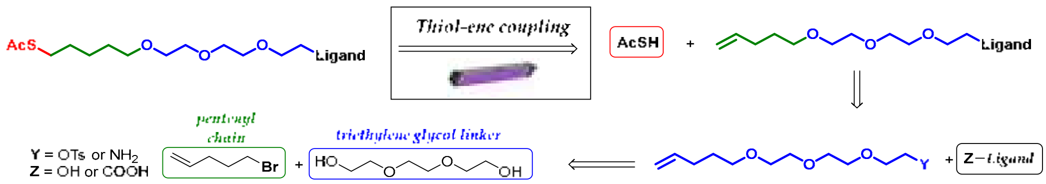

Scheme 1. General retrosynthetic scheme for the preparation of sulfur-functionalized ligands.

Concerning the compound **1** derivative, we decided to connect the linker to the hydroxyl group on the C-6 position of the pyranose ring for two main reasons: firstly, several works suggest that the C6 OH group of D-glucose is not crucial for binding to the SGLT1 interaction and translocation sites [71]; secondly, the primary hydroxyl group is the most easily functionalized among the hydroxyl groups of compound **1**. Hence, to the best of our knowledge, the presence of a linear chain should not affect the biological activity of the molecule. For L-glutamine ligands, we designed two different derivatives bearing, respectively, the TEG-C5 chain on the nitrogen atom of the amide of lateral chain or connecting it directly to the Cα position of the amino acid, with the formation of a new amide group. We decided to synthesize two L-glutamine derivatives with TEG chains linked on two different positions of the aminoacidic structure, lacking information about the binding mode between L-glutamine and B^0AT1 (i.e., which groups are involved in the binding). The preparation of both *C*-glucoside **1** and L-Gln derivatives proceeded to adopt a multistep synthesis, starting from commercially available *O*-Me-α-D-glucopyranoside and protected L-glutamine compounds, as described in Section 3.1.

Once the target ligand compounds were prepared, the experiment consisted of the preparation, purification and characterization of gold nanoparticles (Figure 4) loaded with compound **2**, D-glucose derivative (**GlcC$_5$SH**) and L-glutamine derivatives **4** and **5**, as described in Section 3.2.

3.1. Preparation of Ligands

Concerning the synthesis of compound **2** (i.e., the *C*-glucoside **1** bearing a suitable sulfur-ending linker), the following synthetic steps were carried out (see Scheme 2 which also includes the reaction conditions and yields of each step). Commercially available *O*-Me-α-D-glucopyranoside was subjected to a chemoselective protecting-group-free *C*-allylation according to the procedure described in [60] (compound **6**). After perbenzylation (compound **7**), a successive acetolysis reaction, using a mixture of trifluoroacetic acid and acetic anhydride, allowed for the regioselective replacement of the benzyl protecting group on the C-6 position with an acetyl ester (compound **8**). The allyl handle was then manipulated by firstly oxidizing it into aldehyde **9**, then reducing it to alcohol **10,** and finally converting it into azidoethyl derivative **11** through a Mitsunobu-like reaction. The acetyl group was successively removed from the C6-OH position (compound **12**), which was in turn alkylated with the electrophilic TEG-C5 chain bearing a *p*-toluensulphonate function as leaving group (compound **14**). The tosylate linker **14** spacer was synthesized starting from triethyleneglycol, then monoalkylated with a 4-pentenyl chain (compound **13**) and finally reacted with tosyl chloride. In our first planned synthesis, we subjected compound **15** to BCl_3-promoted benzyl ether deprotection, but we observed the simultaneous cleavage of the polyethyleneglycol chain. Hence, we decided firstly to subject the TEGylated sugar derivative to a radical-mediated reaction. Upon UV exposure at 365 nm and adding DPAP, a radical photoinitiator, the allyl group was converted into thioester **16**. Successively, we attempted to use both catalytic hydrogenolysis and Birch conditions for the azide reduction and benzyl group cleavage, but surprisingly, in both cases, complete removal of the thioester group, generating a pentyl-ending chain, occurred. Indeed, the desulfurization of thioester by SET (single electron transfer) processes is described and rationalized in the literature [72]. Therefore, a change in strategy was needed, so we proceeded with deprotecting the thioester group and promoting its transformation into a disulfide bond to obtain a kind of "protected" thiol derivative (compound **17**). Birch reduction of this compound led to the desired fully deprotected dimer **18**, the two amine functionalities of which were transformed into dansyl-sulfonamides, affording the final dimer **2**. This compound was used directly for the generation of the nanoparticles; it is possible to use both thiol-free and disulfide-bearing molecules, since the addition of an excess of $NaBH_4$ leads to the disulfide bridge reduction.

The synthesis of the L-glutamine derivatives **4** and **5** proceeded with the following steps (Scheme 3). The tosyl group on the C5-TEG chain of compound **14** was converted into the azide functionality (compound **19**), which was reduced to amine derivative **20**. A condensation between this compound and Fmoc-L-Gln-Trt-OH afforded the TEGylated derivative **21**, which was subjected to protecting-group cleavage both in basic and acid conditions, affording the deprotected amino acid derivative **22**. The thiol–ene coupling (TEC) with thioacetic acid gave thioester **23,** which was then converted into the respective dimer **4** (the results was obtained from NMR analysis). The obtained disulfide was directly used for nanoparticle preparation. The condensation of amine **20** with Boc-L-Glu-O-tBu (Boc-L-glutamic acid 1-tert-butyl ester) gave intermediate **24**, which was deprotected by acidic conditions. The successive TEC with thioacetic acid afforded thioester **26**. Then, thioester deprotection with the methanolysis conditions used for compound **4** led to a complex mixture of side products, probably due to the competing deprotonation reaction of the α-carbon on the glutamine residue; this process did not occur for the first aminoacidic derivative since the racemizable carbon atom of the glutamine was located on the α position of the newly formed amide, and not on a carboxylic acid group as in **26**. Hence, we decided to perform the preparation of the nanoparticles using the L-glutamine derivative **4**.

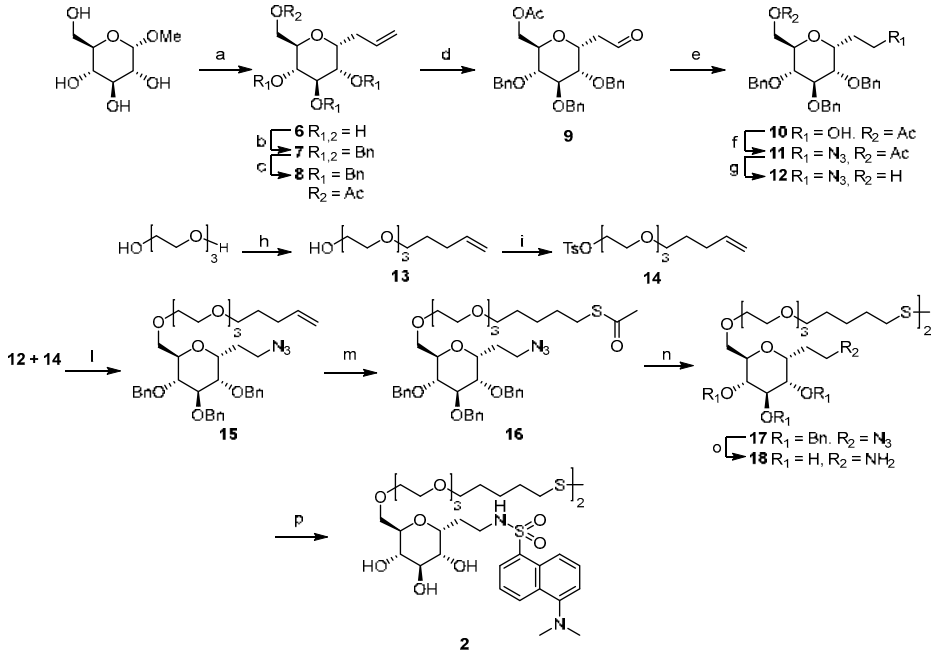

Scheme 2. Reagents and conditions: (a) BSTFA, CH3CN, reflux, 3 h; allyltrimethylsilane, TMSOTf, 0 °C to r.t., 12 h [60]; (b) BnBr, NaH, DMF dry, r.t., 3 h [61]; (c) Ac_2O, TFA, 0 °C, 1 h, 88%; (d) i. O_3, CH_2Cl_2, −78 °C, 1 h; ii. Ph_3P, CH_2Cl_2, −78 °C to r.t., 24 h, 82%; (e) $NaBH_4$, MeOH, 0 °C, 2 h, 95%; (f) DIAD, Ph_3P, $(PhO)_2PON_3$, THF dry, 0 °C to r.t., 2 h, 90%; (g) MeONa, MeOH dry, r.t., 1 h, 95%; (h) 5-Bromo-1-pentene, NaOH, neat, 100 °C, 14 h, 74%; (i) TsCl, Et_3N, DIPEA, CH_2Cl_2, r.t., 3 h, 72%; (l) NaH, DMF dry, r.t., 12 h, 83%; (m) AcSH, DPAP, CH_2Cl_2, r.t., UV light (365 nm), 1 h, 85%; (n) MeONa, MeOH, r.t., 16 h; (o) Na, NH_3(l), THF dry, −78 °C, 15 min, then NH_4Cl, r.t., 65%; (p) dansyl chloride, Et_3N, MeOH, r.t., 5 h, 39%.

The synthesis of the L-glutamine derivatives **4** and **5** proceeded with the following steps (Scheme 3). The tosyl group on the C5-TEG chain of compound **14** was converted into the azide functionality (compound **19**), which was reduced to amine derivative **20**. A condensation between this compound and Fmoc-L-Gln-Trt-OH afforded the TEGylated derivative **21**, which was subjected to protecting-group cleavage both in basic and acid conditions, affording the deprotected amino acid derivative **22**. The thiol–ene coupling (TEC) with thioacetic acid gave thioester **23,** which was then converted into the respective dimer **4** (the results was obtained from NMR analysis). The obtained disulfide was directly used for nanoparticle preparation. The condensation of amine **20** with Boc-L-Glu-O-tBu (Boc-L-glutamic acid 1-tert-butyl ester) gave intermediate **24**, which was deprotected by acidic conditions. The successive TEC with thioacetic acid afforded thioester **26**. Then, thioester deprotection with the methanolysis conditions used for compound **4** led to a complex mixture of side products, probably due to the competing deprotonation reaction of the α-carbon on the glutamine residue; this process did not occur for the first aminoacidic derivative since the racemizable carbon atom of the glutamine was located on the α position of the newly formed amide, and not on a carboxylic acid group as in **26**. Hence, we decided to perform the preparation of the nanoparticles using the L-glutamine derivative **4**.

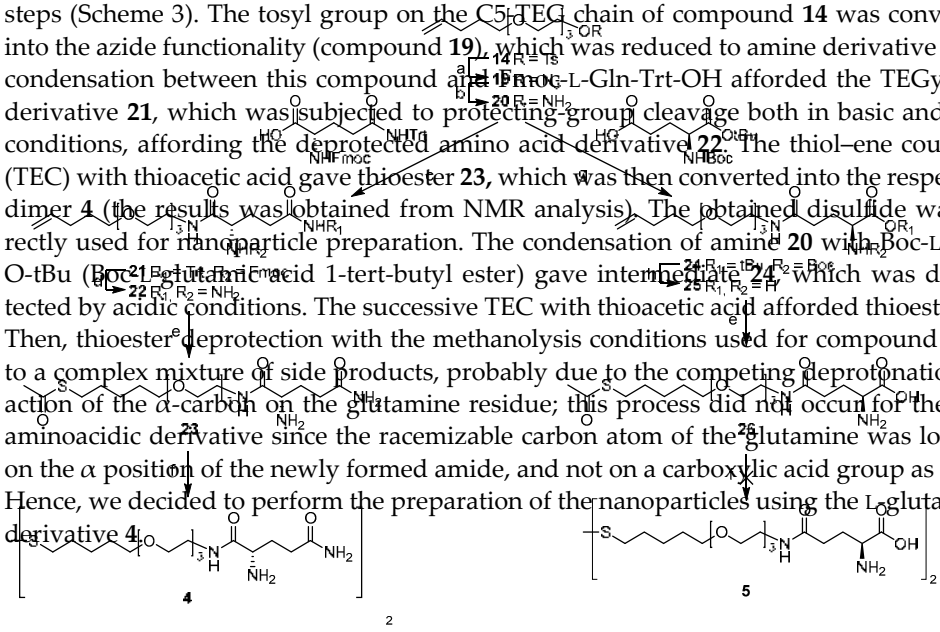

Scheme 3. Reagents and conditions: (a) NaN_3, DMF dry, 80 °C, 48 h, 78%; (b) i. Ph_3P, THF, reflux, 3h; ii. H_2O, r.t., 12 h, 93%; (c) EDC, HOBt, Et_3N, DMF dry, 0 °C to r.t., 12 h, 79%; (d) i. CH_2Cl_2, TFA, r.t., 2 h; ii. piperidine, DMF, r.t., 12 h, 96%; (e) AcSH, DPAP, MeOH, r.t., UV light (365 nm), 1 h, 47% (for 20) and 53% (for 24); (f) MeONa, MeOH, r.t., 2 h; (g) EDC, HOBt, Et_3N, DMF dry, 0 °C to r.t., 12 h, 95%; (h) CH_2Cl_2, TFA, r.t., 2 h, 30%.

3.2. Preparation of the Au Nanoparticles

After completing the synthesis of the ligands of interest, the preparation of four different gold nanoparticles (AuNP1–AuNP4, Figure 5) was carried out by using the disulfide ligands **2** and **4** and the D-glucose derivative *O*-(5′-thiopentyl)-β-D-glucopyranoside (**GlcC$_5$SH**, compound **3**), synthesized according to [65,66].

The preparation of the gold nanoparticles involved a one-pot process, inspired by the methods developed in 1994 by Brust and Schriffin [73], and successively optimized by

3.2. Preparation of the Au Nanoparticles

After completing the synthesis of the ligands of interest, the preparation of four different gold nanoparticles (AuNP1–AuNP4, Figure 5) was carried out by using the disulfide ligands **2** and **4** and the D-glucose derivative *O*-(5′-thiopentyl)-β-D-glucopyranoside (**GlcC$_5$SH**, compound **3**), synthesized according to [65,66].

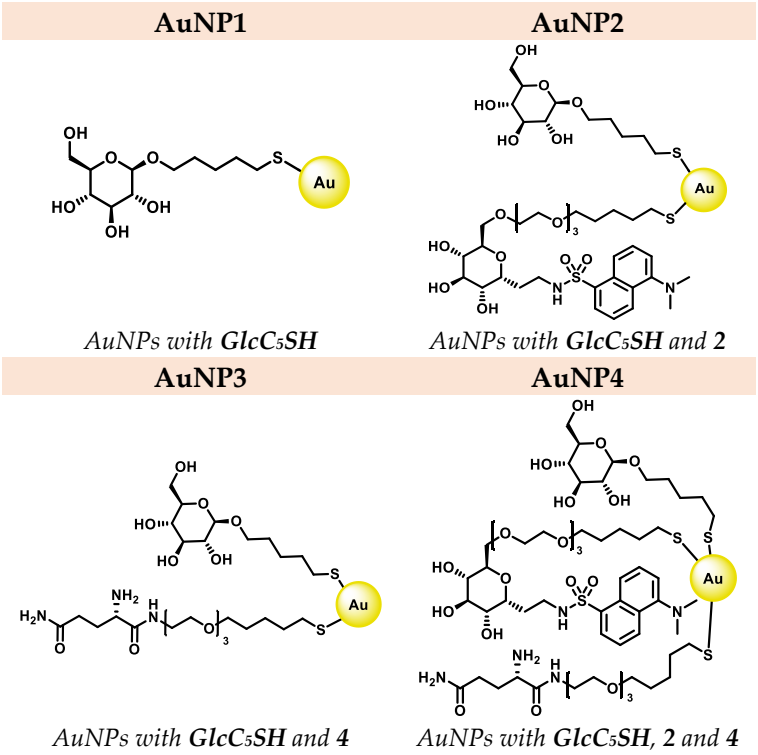

Figure 5. Structure of the four multivalent nanoparticles prepared in this work.

3.3. Nanoparticle Characterization

After dialysis and freeze-drying, the AuNPs were obtained as black powder and could be easily re-dispersed in water without flocculation.

The obtainment of decorated AuNPs with the synthesized ligands was preliminary assessed with infrared spectroscopy. In particular, FT-IR/ATR analyses on solid samples of AuNPs 1–4 were performed (Figure 6). The registered IR spectra on AuNP1–4 showed the presence of several bands associated with the functional groups of the decorating ligands, for example the stretching bands of sugar OH groups around 3300 cm^{-1}, the stretching bands of CH_2 of pentenyl chains at 2900 cm^{-1}, the C-O stretching band of ethylene glycol chains and of sugar rings in the region of 1015 cm^{-1}, as well as bands around 1650 cm^{-1} (stretching of aromatics) and 1350 cm^{-1} (OH bending). The IR spectra of AuNP3 and AuNP4 present a narrow band around 830 cm^{-1} that can be associated with the bending vibrations of the amino group of the glutamine derivative grafted on AuNP 3 and 4.

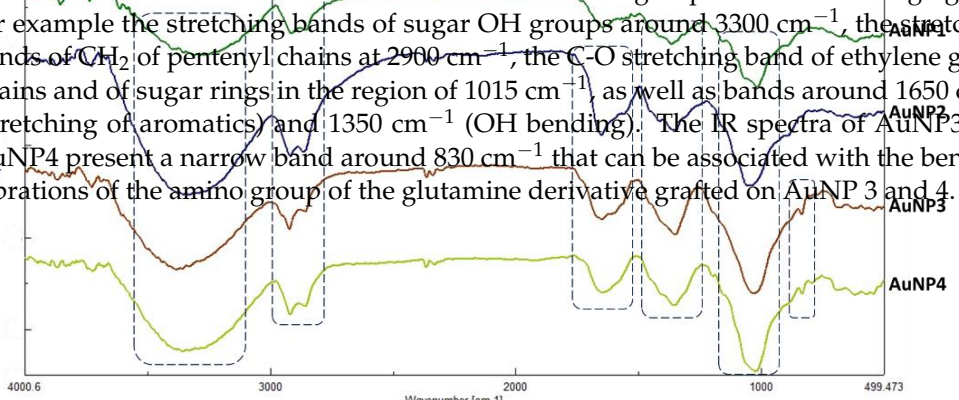

ands, for example the stretching bands of sugar OH groups around 3300 cm^{-1}, the stretching bands of CH_2 of pentenyl chains at 2900 cm^{-1}, the C-O stretching band of ethylene glycol chains and of sugar rings in the region of 1015 cm^{-1}, as well as bands around 1650 cm^{-1} (stretching of aromatics) and 1350 cm^{-1} (OH bending). The IR spectra of AuNP3 and AuNP4 present a narrow band around 830 cm^{-1} that can be associated with the bending vibrations of the amino group of the glutamine derivative grafted on AuNP 3 and 4.

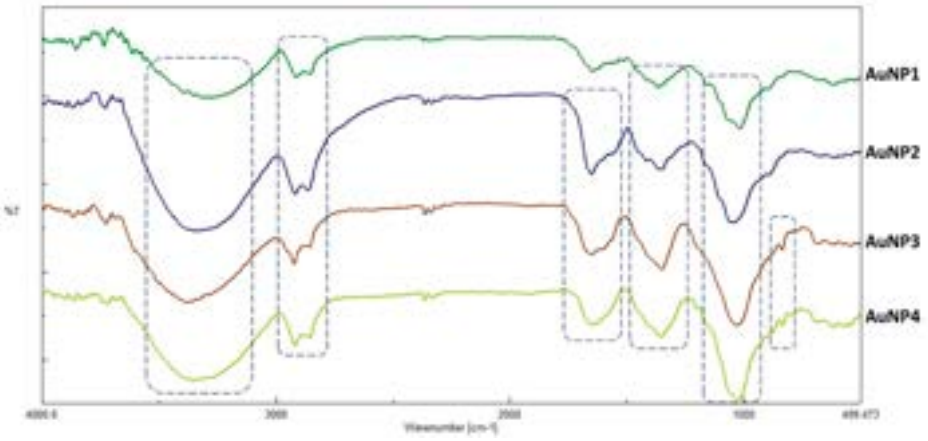

Figure 6. FT-IR/ATR spectra of prepared AuNPs 1–4. Some diagnostic stretching and bending vibrations are circled. Individual IR spectra of AuNP1–4 are reported in the Supporting Information.

Morphological characterization of AuNP1–4 was carried out by TEM (transmission electron microscopy) analysis. The measurement of the AuNPs' size and their distribution was accomplished using *ImageJ* (version 1.54 bundled 64-bit) and *Origin* (version Pro 2023 64-bit SR1) software, adopting the procedure and the processing steps described recently by Zhang and Wang [74]. Except for the AuNP4 sample, for which we counted a little bit less than 100 nanoparticles, in AuNP1, 2 and 3, we counted more than 100 nanoparticles. The four analyzed dispersions revealed the presence of nanoparticles ranging between 2 nm and 6 nm in diameter (gold core), with those of 2 nm being the most representative one, as indicated in the diameter distribution histograms of Table 1.

In order to further confirm the mean size of the AuNPs, the AuNP2 sample was chosen as a model and was subjected to UV–VIS spectroscopy analysis (Figure 7). The nanoparticles were dissolved in water at two different dilutions (0.5 mg/mL and 0.25 mg/mL), and only at the

Morphological characterization of AuNP1–4 was carried out by TEM (transmission electron microscopy) analysis. The measurement of the AuNPs' size and their distribution was accomplished using *ImageJ* (version 1.54 bundled 64-bit) and *Origin* (version Pro 2023 64-bit SR1) software, adopting the procedure and the processing steps described recently by Zhang and Wang [74]. Except for the AuNP4 sample, for which we counted a little bit less than 100 nanoparticles, in AuNP1, 2 and 3, we counted more than 100 nanoparticles. The four analyzed dispersions revealed the presence of nanoparticles ranging between 2 nm and 6 nm in diameter (gold core), with those of 2 nm being the most representative one, as indicated in the diameter distribution histograms of Table 1.

Table 1. TEM micrographs and size (diameter) distribution of the prepared nanoparticles.

Table 1. TEM micrographs and size (diameter) distribution of the prepared nanoparticles.

Nanoparticle	TEM Micrograph	Diameter Distribution Histogram
AuNP1	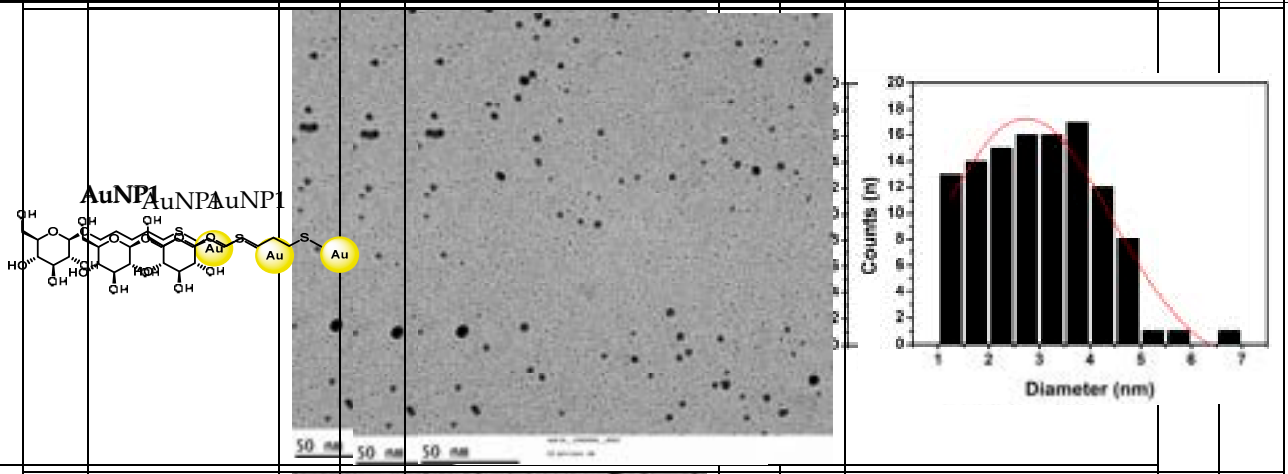	
AuNP2	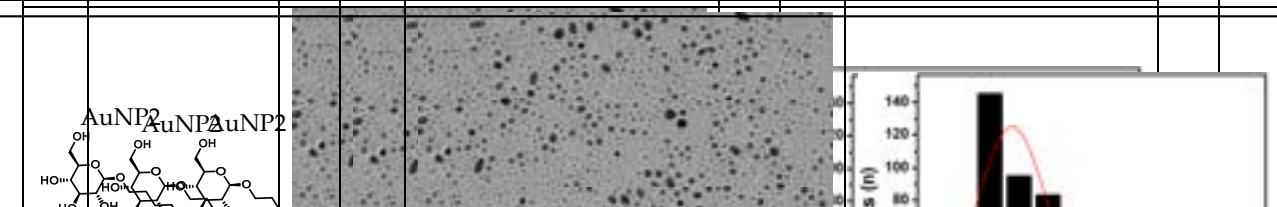	

Nanoparticle	TEM	Diameter Distribution Histogram
AuNP1 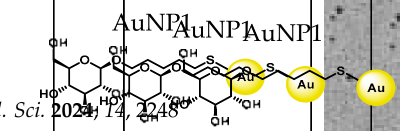	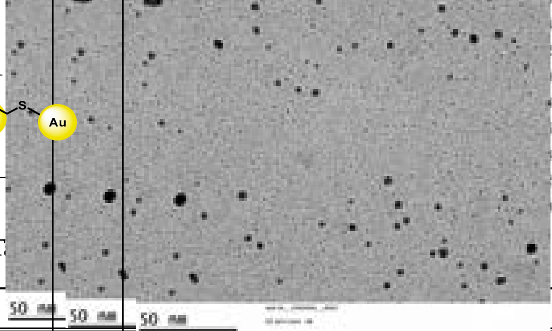	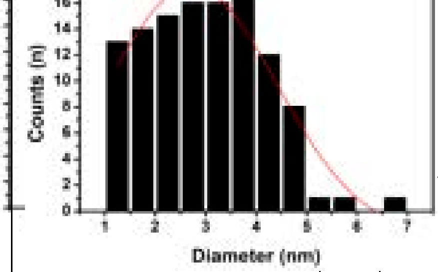
AuNP2 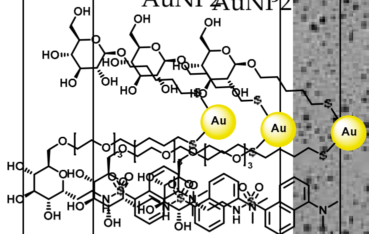	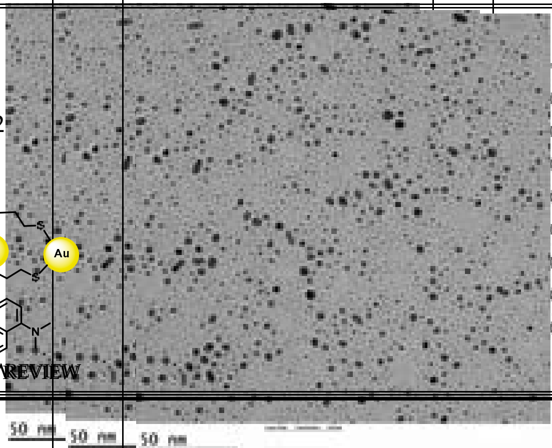	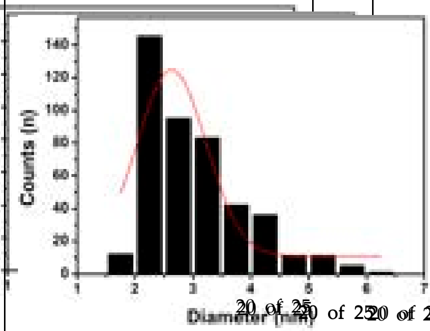
AuNP3 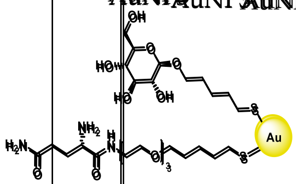	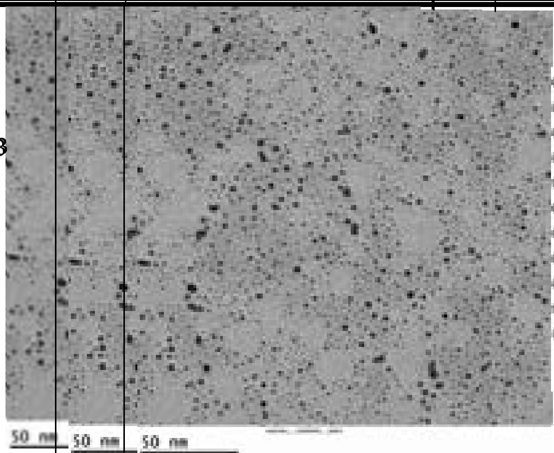	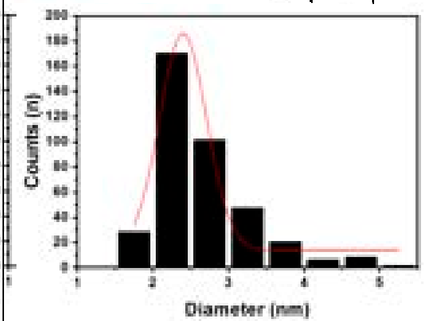
AuNP4 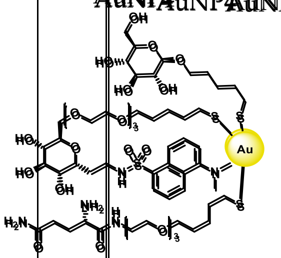	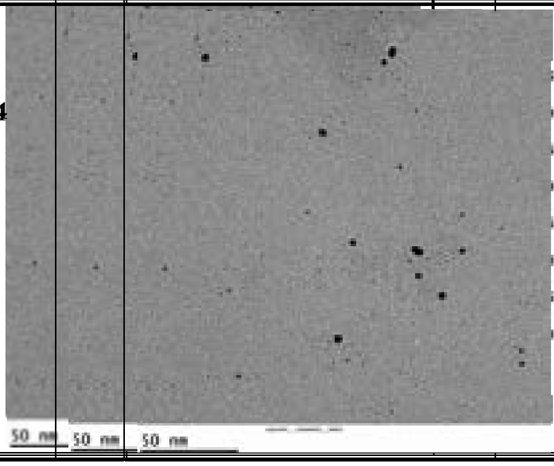	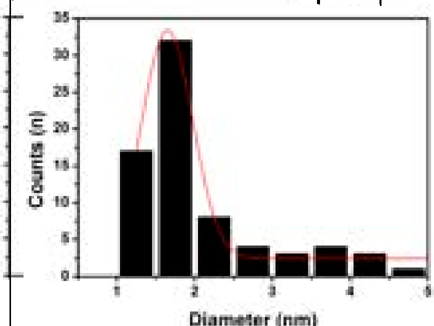

In order to further confirm the mean size of the AuNPs, the AuNP2 sample was chosen as a model and was subjected to UV-Vis spectroscopy analysis (Figure 7). The nanoparticles were dissolved in water at two different dilutions (0.5 mg/mL and 0.25 mg/mL), and only at the higher concentration was it possible to notice a weak plasmonic absorption band around 520 nm, which is correlated to the presence of few nanoparticles with a bigger core diameter.

...spectra show broad signals of the ligands, typical for this kind of nanosystem [64,66]. In particular, signals of D-glucose derivative **GlcC$_5$SH**, *C*-glucoside derivative **2** (in AuNP2) and L-glutamine derivative **4** (in AuNP3) grafted onto a nanosized entity are clearly visible in the respective ^{1}H-NMR spectra (Figure 8A). Before the preparation of the nanoparticles, an ^{1}H-NMR spectrum of a ligand-containing mixture

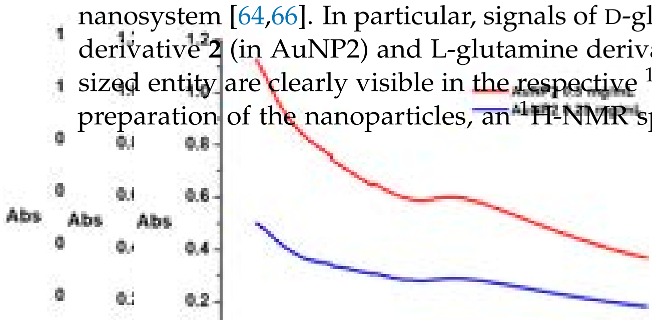

In order to further confirm the mean size of the AuNPs, the AuNP2 sample was chosen as a model and was subjected to UV–VIS spectroscopy analysis (Figure 7). The nanoparticles were dissolved in water at two different dilutions (0.5 mg/mL and 0.25 mg/mL), and only at the higher concentration was it possible to notice a weak plasmon absorption band around 520 nm, which is correlated to the presence of few nanoparticles with a mean diameter of 10 nm.

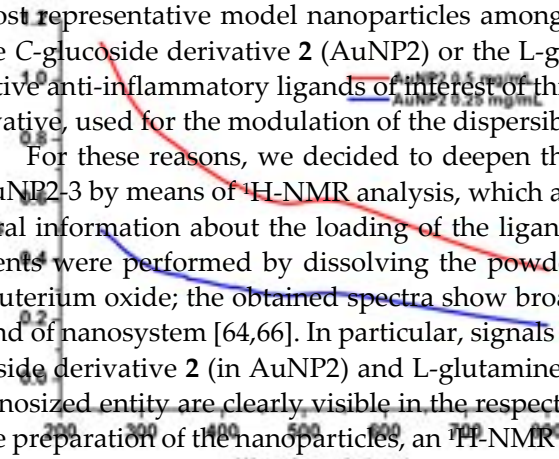

Figure 7. UV–VIS spectrum of AuNP2 dissolved in water. Red line: dilution of 0.5 mg/mL; blue line: dilution of 0.25 mg/mL.

According to the obtained results, AuNP2 and AuNP3 showed the best features in terms of final mass yield and size distribution. Moreover, AuNP2 and AuNP3 were the most representative model nanoparticles among the prepared ones, since they exposed the *C*-glucoside derivative **2** (AuNP2) or the L-glutamine derivative 4 (AuNP3), the two active anti-inflammatory ligands of interest of this work, and the D-glucose **GlcC$_5$SH** derivative, used for the modulation of the dispersibility of the nanoparticles.

For these reasons, we decided to deepen the physical–chemical characterization of AuNP2-3 by means of ^{1}H-NMR analysis, which allowed us to obtain more detailed structural information about the loading of the ligands on the AuNPs. The ^{1}H-NMR experiments were performed by dissolving the powder comprised of AuNP2 and AuNP3 in deuterium oxide; the obtained spectra show broad signals of the ligands, typical for this kind of nanosystem [64,66]. In particular, signals of D-glucose derivative **GlcC$_5$SH**, *C*-glucoside derivative **2** (in AuNP2) and L-glutamine derivative **4** (in AuNP3) grafted onto a nanosized entity are clearly visible in the respective ^{1}H-NMR spectra (Figure 8A). Before the preparation of the nanoparticles, an ^{1}H-NMR spectrum of a ligand-containing mixture was recorded to check the ligands' ratio (Figure 8B); this was compared with the ^{1}H-NMR spectra recorded for the respective AuNPs, allowing for qualitative determination of the loading of the ligands on the NPs.

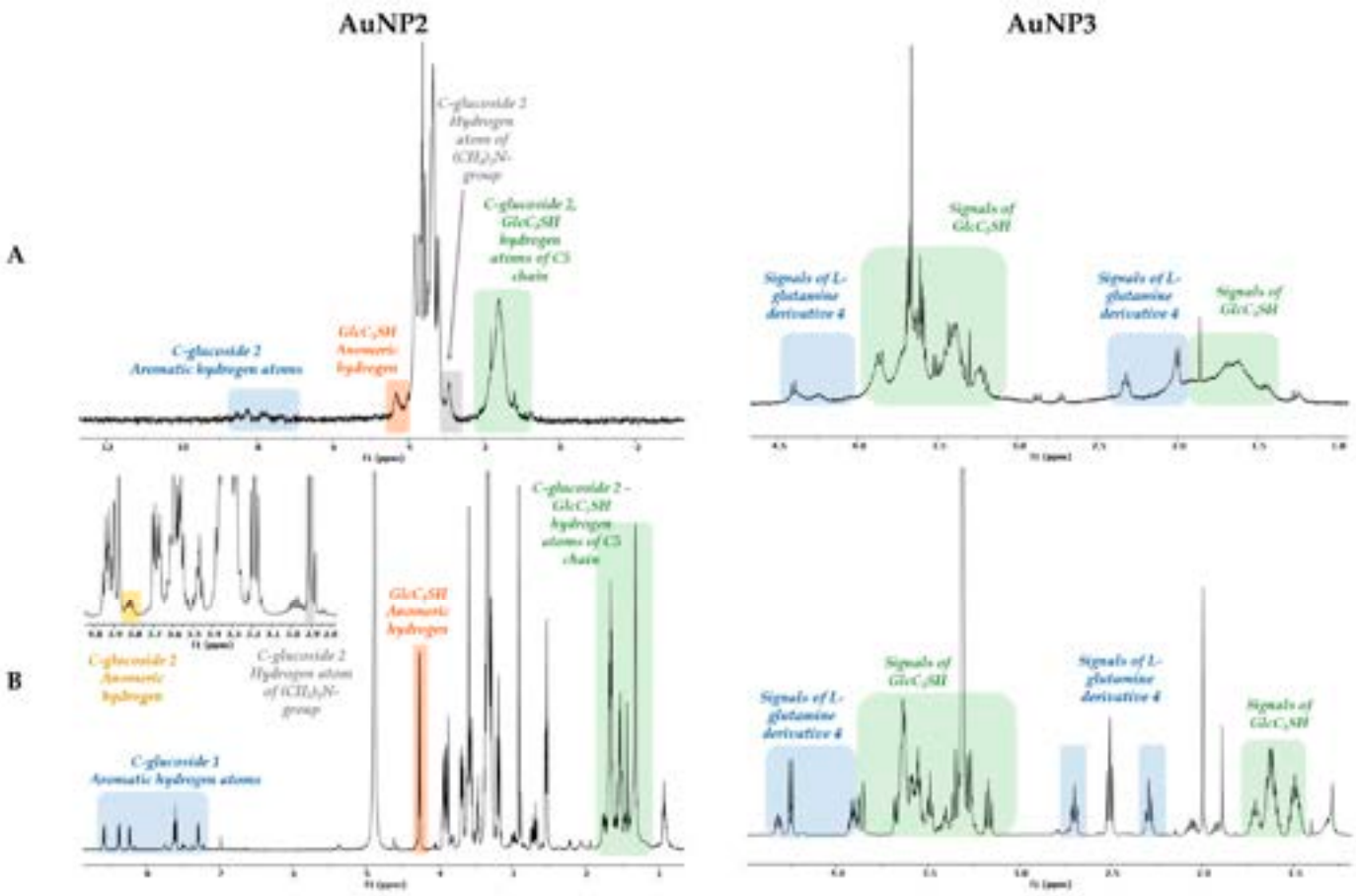

Figure 8. (**A**) ^{1}H-NMR spectra (with water suppression signal sequence) of the final AuNP2 (on the left) and AuNP3 (on the right). (**B**) ^{1}H-NMR spectrum of the solution of **GlcC$_5$SH 3** and *C*-glycoside derivative **2** (in CD_3OD) before AuNP2 preparation (on the left); ^{1}H-NMR spectrum of the solution of **GlcC$_5$SH 3** and L-glutamine derivative **4** (in CD_3OD) before AuNP3 preparation (on the right). Some diagnostic signals are highlighted with different colors.

4. Conclusions

In this work, we presented the design, synthesis and characterization of gold nanoparticles decorated with different compounds, derivatives of D-glucose, *C*-glycoside 1 and L-glutamine. The last two represent active ligands of the co-transporters SGLT1 and B^0AT1, with a protective role against inflammatory agents. The two active compounds were functionalized with a tri(ethylene glycol) chain and a five-carbon spacer with a terminal thiol group to ensure their attachment to the gold nanoparticles, exploiting the affinity between the gold atoms and the thiol groups, and to provide an adequate distance of these molecules from the core of each gold nanoparticle. A glucose derivative, with a pentyl chain bearing a terminal thiol group, was also included to improve the water solubility of the NPs. The obtained AuNPs represent a useful tool to assess the multivalent/synergic activities of the ligands and to unveil the biochemical and physiological mechanisms at the basis of the anti-inflammatory activity correlated with the two co-transporters SGLT1 and B^0AT1.

Supplementary Materials: The following supporting information can be downloaded at: https://www.mdpi.com/article/10.3390/app14062248/s1.

Author Contributions: Conceptualization, G.D., B.L.F. and M.M.; methodology, G.D., B.L.F. and M.M.; writing—original draft preparation, G.D.; writing—review and editing, G.D., B.L.F. and M.M.; supervision, B.L.F. and M.M. All authors have read and agreed to the published version of the manuscript.

Funding: We acknowledge financial support from the European Cooperation in Science and Technology COST Action CM1102—Multivalent Glycosystems for Nanoscience—MultiGlycoNano.

Institutional Review Board Statement: Not applicable.

Informed Consent Statement: Not applicable.

Data Availability Statement: Data are contained within this article or the Supplementary Materials.

Acknowledgments: Soledad Penadés is gratefully acknowledged for hosting G.D. in the laboratory facilities of CIC biomaGUNE (San Sebastián, Spain) within the Short-Term Scientific Mission, financed by COST Action CM1102, and for the general supervision of the research. Part of the NMR analyses were performed at the NMR facility of the Unitech COSPECT at the University of Milan (Italy).

Conflicts of Interest: The authors declare no conflicts of interest.

References

1. Spiljar, M.; Merkler, D.; Trajkovski, M. The Immune System Bridges the Gut Microbiota with Systemic Energy Homeostasis: Focus on TLRs, Mucosal Barrier, and SCFAs. *Front. Immunol.* **2017**, *8*, 1353. [CrossRef] [PubMed]
2. Denning, T.L.; Wang, Y.C.; Patel, S.R.; Williams, I.R.; Pulendran, B. Lamina propria macrophages and dendritic cells differentially induce regulatory and interleukin 17-producing T cell responses. *Nat. Immunol.* **2007**, *8*, 1086–1094. [CrossRef] [PubMed]
3. Zheng, D.; Liwinski, T.; Elinav, E. Interaction between microbiota and immunity in health and disease. *Cell Res.* **2020**, *30*, 492–506. [CrossRef] [PubMed]
4. Nishida, A.; Inoue, R.; Inatomi, O.; Bamba, S.; Naito, Y.; Andoh, A. Gut microbiota in the pathogenesis of inflammatory bowel disease. *Clin. J. Gastroenterol.* **2018**, *11*, 1–10. [CrossRef]
5. Brestoff, J.R.; Artis, D. Commensal bacteria at the interface of host metabolism and the immune system. *Nat. Immunol.* **2013**, *14*, 676–684. [CrossRef]
6. Frank, D.N.; St Amand, A.L.; Feldman, R.A.; Boedeker, E.C.; Harpaz, N.; Pace, N.R. Molecular-phylogenetic characterization of microbial community imbalances in human inflammatory bowel diseases. *Proc. Natl. Acad. Sci. USA* **2007**, *104*, 13780–13785. [CrossRef] [PubMed]
7. Yu, L.C.H.; Flynn, A.N.; Turner, J.R.; Buret, A.G. SGLT-1-mediated glucose uptake protects intestinal epithelial cells against LPS-induced apoptosis and barrier defects: A novel cellular rescue mechanism? *FASEB J.* **2005**, *19*, 1822–1835. [CrossRef]
8. Yu, L.C.H.; Turner, J.R.; Buret, A.G. LPS/CD14 activation triggers SGLT-1-mediated glucose uptake and cell rescue in intestinal epithelial cells via early apoptotic signals upstream of caspase-3. *Exp. Cell Res.* **2006**, *312*, 3276–3286. [CrossRef]
9. Wright, E.M.; Loo, D.D.F.; Hirayama, B.A.; Turk, E. Surprising versatility of Na^+-glucose cotransporters: SLC5. *Physiology* **2004**, *19*, 370–376. [CrossRef]
10. Gorboulev, V.; Schuermann, A.; Vallon, V.; Kipp, H.; Jaschke, A.; Klessen, D.; Friedrich, A.; Scherneck, S.; Rieg, T.; Cunard, R.; et al. Na+-D-glucose Cotransporter SGLT1 is Pivotal for Intestinal Glucose-Absorption and Glucose-Dependent Incretin Secretion. *Diabetes* **2012**, *61*, 187–196. [CrossRef]

11. Koepsell, H. Glucose transporters in the small intestine in health and disease. *Pflug. Arch-Eur. J. Physiol.* **2020**, *472*, 1207–1248. [CrossRef]
12. Palazzo, M.; Gariboldi, S.; Zanobbio, L.; Selleri, S.; Dusio, G.F.; Mauro, V.; Rossini, A.; Balsari, A.; Rumio, C. Sodium-dependent glucose transporter-1 as a novel immunological player in the intestinal mucosa. *J. Immunol.* **2008**, *181*, 3126–3136. [CrossRef]
13. Zanobbio, L.; Palazzo, M.; Gariboldi, S.; Dusio, G.F.; Cardani, D.; Mauro, V.; Marcucci, F.; Balsari, A.; Rumio, C. Intestinal Glucose Uptake Protects Liver from Lipopolysaccharide and D-Galactosamine, Acetaminophen, and Alpha-Amanitin in Mice. *Am. J. Pathol.* **2009**, *175*, 1066–1076. [CrossRef] [PubMed]
14. La Ferla, B.; Spinosa, V.; D'Orazio, G.; Palazzo, M.; Balsari, A.; Foppoli, A.A.; Rumio, C.; Nicotra, F. Dansyl C-glucoside as a novel agent against endotoxic shock. *ChemMedChem* **2010**, *5*, 1677–1680. [CrossRef]
15. Cardani, D.; Sardi, C.; La Ferla, B.; D'Orazio, G.; Sommariva, M.; Marcucci, F.; Olivero, D.; Tagliabue, E.; Koepsell, H.; Nicotra, F.; et al. Sodium glucose cotransporter 1 ligand BLF501 as a novel tool for management of gastrointestinal mucositis. *Mol. Cancer* **2014**, *13*, 23. [CrossRef]
16. Cetinbas, F.; Yelken, B.; Gulbas, Z. Role of glutamine administration on cellular immunity after total parenteral nutrition enriched with glutamine in patients with systemic inflammatory response syndrome. *J. Crit. Care* **2010**, *25*, 661.e1–661.e6. [CrossRef]
17. Alonso Pérez, L.; Fernández Vázquez, A.; Valero Zanuy, M.A.; Gomis Muñoz, P.; León Sanz, M.; Herreros de Tejada, A. Parenteral nutrition supplemented with glutamine in patients undergoing bone marrow transplantation. *Nutr. Hosp.* **2010**, *25*, 49–52. [PubMed]
18. Estívariz, C.F.; Griffith, D.P.; Luo, M.; Szeszycki, E.E.; Bazargan, N.; Dave, N.; Daignault, N.M.; Bergman, G.F.; McNally, T.; Battey, C.H.; et al. Efficacy of parenteral nutrition supplemented with glutamine dipeptide to decrease hospital infections in critically ill surgical patients. *J. Parenter. Enter. Nutr.* **2008**, *32*, 389–402. [CrossRef] [PubMed]
19. Fillmann, H.; Kretzmann, N.A.; San-Miguel, B.; Llesuy, S.; Marroni, N.; Gonzalez-Gallego, J.; Tunon, M.J. Glutamine inhibits over-expression of pro-inflammatory genes and down-regulates the nuclear factor kappaB pathway in an experimental model of colitis in the rat. *Toxicology* **2007**, *236*, 217–226. [CrossRef]
20. Huang, Y.; Li, N.; Liboni, K.; Neu, J. Glutamine decreases lipopolysaccharide-induced IL-8 production in Caco-2 cells through a non-NF-kappa B p50 mechanism. *Cytokine* **2003**, *22*, 77–83. [CrossRef]
21. Sukhotnik, I.; Mogilner, J.G.; Karry, R.; Shamian, B.; Lurie, M.; Kokhanovsky, N.; Ure, B.M.; Coran, A.G. Effect of oral glutamine on enterocyte turnover during methotrexate-induced mucositis in rats. *Digestion* **2009**, *79*, 5–13. [CrossRef]
22. Choi, K.; Lee, S.S.; Oh, S.J.; Lim, S.Y.; Jeon, W.K.; Oh, T.Y.; Kim, J.W. The effect of oral glutamine on 5-fluorouracil/leucovorin-induced mucositis/stomatitis assessed by intestinal permeability test. *Clin. Nutr.* **2007**, *26*, 57–62. [CrossRef] [PubMed]
23. Sukhotnik, I.; Pollak, Y.; Coran, A.G.; Pilatov, J.; Bejar, J.; Mogilner, J.G.; Berkowitz, D. Glutamine attenuates the inhibitory effect of methotrexate on TLR signaling during intestinal chemotherapy-induced mucositis in a rat. *Nutr. Metab.* **2014**, *11*, 17. [CrossRef] [PubMed]
24. Sukhotnik, I.; Agam, M.; Shamir, R.; Shehadeh, N.; Lurie, M.; Coran, A.G.; Shiloni, E.; Mogilner, J. Oral glutamine prevents gut mucosal injury and improves mucosal recovery following lipopolysaccharide endotoxemia in a rat. *J. Surg. Res.* **2007**, *143*, 379–384. [CrossRef] [PubMed]
25. Nose, S.; Wasa, M.; Tazuke, Y.; Owari, M.; Fukuzawa, M. Cisplatin upregulates glutamine transport in human intestinal epithelial cells: The protective mechanism of glutamine on intestinal mucosa after chemotherapy. *J. Parenter. Enter. Nutr.* **2010**, *34*, 530–537. [CrossRef]
26. Tazuke, Y.; Maeda, K.; Wasa, M.; Satoko, N.; Fukuzawa, M. Protective mechanism of glutamine on the expression of proliferating cell nuclear antigen after cisplatin-induced intestinal mucosal injury. *Pediatr. Surg. Int.* **2011**, *27*, 151–158. [CrossRef] [PubMed]
27. Talukder, J.R.; Kekuda, R.; Saha, P.; Arthur, S.; Sundaram, U. Identification and characterization of rabbit small intestinal villus cell brush border membrane Na-glutamine cotransporter. *Am. J. Physiol. Gastrointest. Liver Physiol.* **2008**, *295*, G7–G15. [CrossRef] [PubMed]
28. Saha, P.; Arthur, S.; Kekuda, R.; Sundaram, U. Na-glutamine co-transporters B(0)AT1 in villus and SN2 in crypts are differentially altered in chronically inflamed rabbit intestine. *Biochim. Biophys. Acta* **2012**, *1818*, 434–442. [CrossRef]
29. Melichar, B.; Dvorák, J.; Hyspler, R.; Zadák, Z. Intestinal permeability in the assessment of intestinal toxicity of cytotoxic agents. *Chemotherapy* **2005**, *51*, 336–338. [CrossRef]
30. Weng, X.H.; Beyenbach, K.W.; Quaroni, A. Cultured monolayers of the dog jejunum with the structural and functional properties resembling the normal epithelium. *Am. J. Physiol. Gastrointest. Liver Physiol.* **2005**, *288*, G705–G717. [CrossRef]
31. Ikari, A.; Nakano, M.; Suketa, Y.; Harada, H.; Takagi, K. Reorganization of ZO-1 by sodium-dependent glucose transporter activation after heat stress in LLC-PK1 cells. *J. Cell. Physiol.* **2005**, *203*, 471–478. [CrossRef]
32. Turner, J.R.; Rill, B.K.; Carlson, S.L.; Carnes, D.; Kerner, R.; Mrsny, R.J.; Madara, J.L. Physiological regulation of epithelial tight junctions is associated with myosin light-chain phosphorylation. *Am. J. Physiol.* **1997**, *273*, C1378–C1385. [CrossRef]
33. Li, N.; Neu, J. Glutamine Deprivation Alters Intestinal Tight Junctions via a PI3-K/Akt Mediated Pathway in Caco-2 Cells. *J. Nutr.* **2009**, *139*, 710–714. [CrossRef]
34. Li, N.; Lewis, P.; Samuelson, D.; Liboni, K.; Neu, J. Glutamine regulates Caco-2 cell tight junction proteins. *Am. J. Physiol. -Gastrointest. Liver Physiol.* **2004**, *287*, G726–G733. [CrossRef]

35. Ikari, A.; Nagatani, Y.; Tsukimoto, M.; Harada, H.; Miwa, M.; Takagi, K. Sodium-dependent glucose transporter reduces peroxynitrite and cell injury caused by cisplatin in renal tubular epithelial cells. *Biochim. Biophys. Acta* **2005**, *1717*, 109–117. [CrossRef]
36. Giudicelli, J.; Bertrand, M.F.; Bilski, S.; Tran, T.T.; Poiree, J.C. Effect of cross-linkers on the structure and function of pig-renal sodium-glucose cotransporters after papain treatment. *Biochem. J.* **1998**, *330*, 733–736. [CrossRef]
37. Stevens, B.R.; Fernandez, A.; Hirayama, B.; Wright, E.M.; Kempner, E.S. Intestinal brush-border membrane na+/glucose cotransporter functions insitu as a homotetramer. *Proc. Natl. Acad. Sci. USA* **1990**, *87*, 1456–1460. [CrossRef] [PubMed]
38. Takahashi, M.; Malathi, P.; Preiser, H.; Jung, C.Y. Radiation inactivation studies on the rabbit kidney sodium-dependent glucose transporter. *J. Biol. Chem.* **1985**, *260*, 551–556. [CrossRef]
39. Turner, R.J.; Kempner, E.S. Radiation inactivation studies of the renal brush-border membrane phlorizin-binding protein. *J. Biol. Chem.* **1982**, *257*, 794–797. [CrossRef]
40. Romeo, E.; Dave, M.H.; Bacic, D.; Ristic, Z.; Camargo, S.M.R.; Loffing, J.; Wagner, C.A.; Verrey, F. Luminal kidney and intestine SLC6 amino acid transporters of B(0)AT-cluster and their tissue distribution in Mus musculus. *Am. J. Physiol. Ren. Physiol.* **2006**, *290*, F376–F383. [CrossRef] [PubMed]
41. Mammen, M.; Choi, S.K.; Whitesides, G.M. Polyvalent interactions in biological systems: Implications for design and use of multivalent ligands and inhibitors. *Angew. Chem. Int. Ed.* **1998**, *37*, 2755–2794. [CrossRef]
42. Haag, R. Multivalency as a chemical organization and action principle. *Beilstein J. Org. Chem.* **2015**, *11*, 848–849. [CrossRef]
43. Saha, K.; Agasti, S.S.; Kim, C.; Li, X.; Rotello, V.M. Gold nanoparticles in chemical and biological sensing. *Chem. Rev.* **2012**, *112*, 2739–2779. [CrossRef] [PubMed]
44. Yeh, Y.C.; Creran, B.; Rotello, V.M. Gold nanoparticles: Preparation, properties, and applications in bionanotechnology. *Nanoscale* **2012**, *4*, 1871–1880. [CrossRef] [PubMed]
45. Baram-Pinto, D.; Shukla, S.; Gedanken, A.; Sarid, R. Inhibition of HSV-1 attachment, entry, and cell-to-cell spread by functionalized multivalent gold nanoparticles. *Small* **2010**, *6*, 1044–1050. [CrossRef] [PubMed]
46. Cagno, V.; Andreozzi, P.; D'Alicarnasso, M.; Jacob Silva, P.; Mueller, M.; Galloux, M.; Le Goffic, R.; Jones, S.T.; Vallino, M.; Hodek, J.; et al. Broad-spectrum non-toxic antiviral nanoparticles with a virucidal inhibition mechanism. *Nat. Mater.* **2018**, *17*, 195–203. [CrossRef] [PubMed]
47. Giljohann, D.A.; Seferos, D.S.; Daniel, W.L.; Massich, M.D.; Patel, P.C.; Mirkin, C.A. Gold Nanoparticles for Biology and Medicine. In *Spherical Nucleic Acids*; Mirkin, C.A., Ed.; Jenny Stanford Publishing: New York, NY, USA, 2020. [CrossRef]
48. Liz-Marzán, L.M. Gold nanoparticle research before and after the Brust-Schiffrin method. *Chem. Commun.* **2013**, *49*, 16–18. [CrossRef]
49. Marradi, M.; García, I.; Penadés, S. Carbohydrate-based nanoparticles for potential applications in medicine. *Prog. Mol. Biol. Transl. Sci.* **2011**, *104*, 141–173. [CrossRef]
50. Marradi, M.; Chiodo, F.; Garcia, I. Glyconanotechnology and Disease: Gold Nanoparticles Coated with Glycosides as Multivalent Systems for Potential Applications in Diagnostics and Therapy. *Carbohydr. Drug Des. Discov.* **2015**, *43*, 89–131.
51. Matassini, C.; Marradi, M.; Cardona, F.; Parmeggiani, C.; Robina, I.; Moreno-Vargas, A.J.; Penades, S.; Goti, A. Gold nanoparticles are suitable cores for building tunable iminosugar multivalency. *RSC Adv.* **2015**, *5*, 95817–95822. [CrossRef]
52. Baker, A.N.; Hawker-Bond, G.W.; Georgiou, P.G.; Dedola, S.; Field, R.A.; Gibson, M.I. Glycosylated gold nanoparticles in point of care diagnostics: From aggregation to lateral flow. *Chem. Soc. Rev.* **2022**, *51*, 7238–7259. [CrossRef] [PubMed]
53. Chiodo, F.; Marradi, M.; Tefsen, B.; Snippe, H.; van Die, I.; Penadés, S. High sensitive detection of carbohydrate binding proteins in an ELISA-solid phase assay based on multivalent glyconanoparticles. *PLoS ONE* **2013**, *8*, e73027. [CrossRef]
54. de la Fuente, J.M.; Barrientos, A.G.; Rojas, T.C.; Rojo, J.; Canada, J.; Fernandez, A.; Penades, S. Gold glyconanoparticles as water-soluble polyvalent models to study carbohydrate interactions. *Angew. Chem. Int. Ed.* **2001**, *40*, 2257–2261. [CrossRef]
55. Marradi, M.; Chiodo, F.; Garcia, I.; Penades, S. Glyconanoparticles as multifunctional and multimodal carbohydrate systems. *Chem. Soc. Rev.* **2013**, *42*, 4728–4745. [CrossRef] [PubMed]
56. Buco, F.; Matassini, C.; Vanni, C.; Clemente, F.; Paoli, P.; Carozzini, C.; Beni, A.; Cardona, F.; Goti, A.; Moya, S.E.; et al. Gold nanoparticles decorated with monosaccharides and sulfated ligands as potential modulators of the lysosomal enzyme. *Org. Biomol. Chem.* **2023**, *21*, 9362–9371. [CrossRef] [PubMed]
57. Compostella, F.; Pitirollo, O.; Silvestri, A.; Polito, L. Glyco-gold nanoparticles: Synthesis and applications. *Beilstein J. Org. Chem.* **2017**, *13*, 1008–1021. [CrossRef]
58. Mateu Ferrando, R.; Lay, L.; Polito, L. Gold nanoparticle-based platforms for vaccine development. *Drug Discov. Today Technol.* **2020**, *38*, 57–67. [CrossRef]
59. Terán-Navarro, H.; Zeoli, A.; Salines-Cuevas, D.; Marradi, M.; Montoya, N.; Gonzalez-Lopez, E.; Ocejo-Vinyals, J.G.; Dominguez-Esteban, M.; Gutierrez-Baños, J.L.; Campos-Juanatey, F.; et al. Gold Glyconanoparticles Combined with 91–99 Peptide of the Bacterial Toxin, Listeriolysin O, Are Efficient Immunotherapies in Experimental Bladder Tumors. *Cancers* **2022**, *14*, 2413. [CrossRef]
60. Cardona, F.; La Ferla, B. Synthesis of C-glycoconjugates from readily available unprotected C-allyl glycosides by chemoselective ligation. *J. Carbohydr. Chem.* **2008**, *27*, 203–213. [CrossRef]
61. McGarvey, G.J.; LeClair, C.A.; Schmidtmann, B.A. Studies on the Stereoselective Synthesis of C-Allyl Glycosides. *Org. Lett.* **2008**, *10*, 4727–4730. [CrossRef]

62. Svarovsky, S.A.; Szekely, Z.; Barchi, J.J. Synthesis of gold nanoparticles bearing the Thomsen–Friedenreich disaccharide: A new multivalent presentation of an important tumor antigen. *Tetrahedron Asymmetry* **2005**, *16*, 587–598. [CrossRef]
63. Dettmann, R.; Ziegler, T. Synthesis of octyl S-glycosides of tri- to pentasaccharide fragments related to the GPI anchor of Trypanosoma brucei. *Carbohydr. Res.* **2011**, *346*, 2348–2361. [CrossRef]
64. Martinez-Avila, O.; Hijazi, K.; Marradi, M.; Clavel, C.; Campion, C.; Kelly, C.; Penades, S. Gold Manno-Glyconanoparticies: Multivalent Systems to Block HIV-1 gp120 Binding to the Lectin DC-SIGN. *Chem. A Eur. J.* **2009**, *15*, 9874–9888. [CrossRef]
65. Buskas, T.; Söderberg, E.; Konradsson, P.; Fraser-Reid, B. Use of n-Pentenyl Glycosides as Precursors to Various Spacer Functionalities. *J. Org. Chem.* **2000**, *65*, 958–963. [CrossRef] [PubMed]
66. Barrientos, Á.G.; de la Fuente, J.M.; Rojas, T.C.; Fernández, A.; Penadés, S. Gold Glyconanoparticles: Synthetic Polyvalent Ligands Mimicking Glycocalyx-Like Surfaces as Tools for Glycobiological Studies. *Chem. Eur. J.* **2003**, *9*, 1909–1921. [CrossRef] [PubMed]
67. Zalipsky, S. Chemistry of polyethylene-glycol conjugates with biologically-active molecules. *Adv. Drug Deliv. Rev.* **1995**, *16*, 157–182. [CrossRef]
68. Veronese, F.M.; Pasut, G. PEGylation, successful approach to drug delivery. *Drug Discov. Today* **2005**, *10*, 1451–1458. [CrossRef] [PubMed]
69. Zona, C.; D'Orazio, G.; La Ferla, B. Controlled-Length Efficient Synthesis of Heterobifunctionalized Oligo Ethylene Glycols. *Synlett* **2013**, *24*, 709–712. [CrossRef]
70. Dondoni, A. The Emergence of Thiol–Ene Coupling as a Click Process for Materials and Bioorganic Chemistry. *Angew. Chem. Int. Ed.* **2008**, *47*, 8995–8997. [CrossRef] [PubMed]
71. Tyagi, N.K.; Kumar, A.; Goyal, P.; Pandey, D.; Siess, W.; Kinne, R.R.H. D-Glucose-recognition and phlorizin-binding sites in human sodium/D-glucose cotransporter 1 (hSGLT1): A tryptophan scanning study. *Biochemistry* **2007**, *46*, 13616–13628. [CrossRef] [PubMed]
72. Wang, A.; Hendel, J.; Auzanneau, F.-I. Convergent syntheses of Le(X) analogues. *Beilstein J. Org. Chem.* **2010**, *6*, 17. [CrossRef] [PubMed]
73. Brust, M.; Walker, M.; Bethell, D.; Schiffrin, D.J.; Whyman, R.Y. Synthesis of thiol-derivatised gold nanoparticles in a two-phase Liquid–Liquid system. *J. Chem. Soc. Chem. Commun.* **1994**, *7*, 801. [CrossRef]
74. Zhang, S.; Wang, C. Precise Analysis of Nanoparticle Size Distribution in TEM Image. *Methods Protoc.* **2023**, *6*, 63. [CrossRef] [PubMed]